Inorganic Chemistry

Article

pubs.acs.org/IC

Phosphodiester Cleavage Properties of Copper(II) Complexes of 1,4,7-Triazacyclononane Ligands Bearing Single Alkyl Guanidine Pendants

Linda Tjioe,[†] Tanmaya Joshi,[†] Craig M. Forsyth,[†] Boujemaa Moubaraki,[†] Keith S. Murray,[†] Joël Brugger,[‡,§] Bim Graham,*[,∥] and Leone Spiccia*[,†]

[†]School of Chemistry, Monash University, Vic 3800, Australia

[‡]School of Earth and Environmental Sciences, Centre of Tectonics, Resources and Exploration (TRaX), The University of Adelaide, North Terrace, SA 5005, Australia

[§]Department of Mineralogy, South Australian Museum, Adelaide, SA 5000, Australia

[∥]Medicinal Chemistry and Drug Action, Monash Institute of Pharmaceutical Sciences, Monash University, Parkville, Vic 3052, Australia

Supporting Information

ABSTRACT: Three new metal-coordinating ligands, L^1·4HCl [1-(2-guanidinoethyl)-1,4,7-triazacyclononane tetrahydrochloride], L^2·4HCl [1-(3-guanidinopropyl)-1,4,7-triazacyclononane tetrahydrochloride], and L^3·4HCl [1-(4-guanidinobutyl)-1,4,7-triazacyclononane tetrahydrochloride], have been prepared via the selective N-functionalization of 1,4,7-triazacyclononane (tacn) with ethylguanidine, propylguanidine, and butylguanidine pendants, respectively. Reaction of L^1·4HCl with $Cu(ClO_4)_2·6H_2O$ in basic aqueous solution led to the crystallization of a monohydroxo-bridged binuclear copper(II) complex, $[Cu_2L^1_2(\mu\text{-}OH)](ClO_4)_3·H_2O$ (**C1**), while for L^2 and L^3, mononuclear complexes of composition $[Cu(L^2H)Cl_2]Cl·(MeOH)_{0.5}·(H_2O)_{0.5}$ (**C2**) and $[Cu(L^3H)Cl_2]$-$Cl·(DMF)_{0.5}·(H_2O)_{0.5}$ (**C3**) were crystallized from methanol and DMF solutions, respectively. X-ray crystallography revealed that in addition to a tacn ring from L^1 ligand, each copper(II) center in **C1** is coordinated to a neutral guanidine pendant. In contrast, the guanidinium pendants in **C2** and **C3** are protonated and extend away from the Cu(II)−tacn units. Complex **C1** features a single μ-hydroxo bridge between the two copper(II) centers, which mediates strong antiferromagnetic coupling between the metal centers. Complexes **C2** and **C3** cleave two model phosphodiesters, *bis*(*p*-nitrophenyl)phosphate (BNPP) and 2-hydroxypropyl-*p*-nitrophenylphosphate (HPNPP), more rapidly than **C1**, which displays similar reactivity to $[Cu(tacn)(OH_2)_2]^{2+}$. All three complexes cleave supercoiled plasmid DNA (pBR 322) at significantly faster rates than the corresponding *bis*(alkylguanidine) complexes and $[Cu(tacn)(OH_2)_2]^{2+}$. The high DNA cleavage rate for **C1** {k_{obs} = 1.30 (±0.01) × 10^{-4} s^{-1} vs 1.23 (±0.37) × 10^{-5} s^{-1} for $[Cu(tacn)(OH_2)_2]^{2+}$ and 1.58 (±0.05) × 10^{-5} s^{-1} for the corresponding *bis*(ethylguanidine) analogue} indicates that the coordinated guanidine group in **C1** may be displaced to allow for substrate binding/activation. Comparison of the phosphate ester cleavage properties of complexes **C1**−**C3** with those of related complexes suggests some degree of cooperativity between the Cu(II) centers and the guanidinium groups.

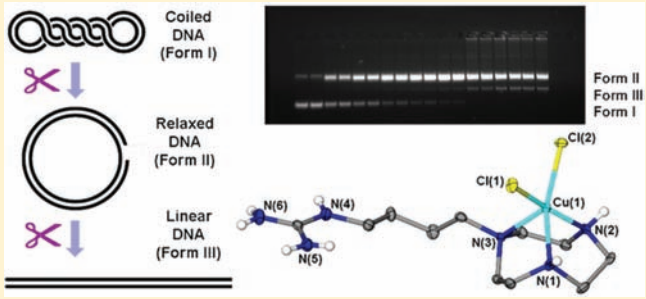

INTRODUCTION

A prominent area of research in coordination chemistry in recent decades has been the development of low molecular weight metal complexes that mimic the function of (ribo)-nuclease and phosphatase metallo-enzymes.[1−7] These studies have sought to improve our knowledge of how these enzymes work, as well as lend understanding to basic metal ion reactivity. The development of complexes as "artificial nucleases" has also been stimulated by realization that hydrolytically active metal complexes (and their conjugates with various targeting agents) may potentially find utility as robust, versatile replacements for restriction enzymes in molecular biology research and as nucleic acid-targeting therapeutics.[8−28]

In the quest to generate cleavage agents with improved reactivity, structural elaboration of simple metal chelates to include auxiliary groups that complement the hydrolytic action of the metal ion(s) has been undertaken.[26,29−42] Inspiration for these designs comes from the enzymes themselves, which, in addition to metal ions, contain amino acid residues at their active sites that assist catalysis by activating the substrate,

Received: September 9, 2011
Published: December 22, 2011

promoting protonation/deprotonation processes, and stabilizing transition states.[43,44] A good example is provided by the well-studied enzyme, alkaline phosphatase (AP), which uses two zinc centers, in conjunction with serine and arginine residues, to promote the rapid cleavage of phosphate monoesters.[45] The positively charged guanidinium group present in arginine is postulated to assist with substrate activation and transition state stabilization, while the serine residue provides the attacking nucleophile, leading to the formation of a phosphoseryl intermediate during the AP catalytic cycle.

Complexes of ligands derived from the facially coordinating macrocycle, 1,4,7-triazacyclononane (tacn), have featured prominently in studies aimed at mimicking metallo-nuclease and -phosphatase function. Pioneering work by Burstyn and coworkers demonstrated that the copper(II)−tacn complex is capable of promoting the cleavage-activated phosphate esters, DNA, RNA, and peptides.[1] Building on these seminal findings, a number of research groups, including our own, have shown that N-functionalization of tacn with various groups can enhance cleavage rates.[28,46−48] Most recently, we reported two series of tacn derivatives with appended guanidinium pendant groups and their copper(II) complexes as nuclease mimics.[49,50] Some evidence for cooperativity between the copper(II) centers and the guanidine pendants was obtained for selected complex−substrate combinations, but the enhancements in reaction rates were modest relative to the non-functionalized complex $[Cu(tacn)(OH_2)_2]^{2+}$. Most notably, a complex incorporating a pair of propyl-linked guanidinium groups was significantly more active than $[Cu(tacn)(OH_2)_2]^{2+}$ in accelerating the cleavage of *bis*(*p*-nitrophenyl)phosphate (BNPP) and 2-hydroxypropyl-*p*-nitrophenylphosphate (HPNPP) but only marginally more active in hydrolyzing plasmid DNA, possibly due to unfavorable steric interactions with the double-helix structure.[49] On the other hand, a series of complexes with single xylyl guanidinium pendants exhibited much higher rates of nuclease cleavage than $[Cu(tacn)(OH_2)_2]^{2+}$ but were on par in terms of their BNPP and HPNPP reactivity.[50] This was interpreted as evidence that the more rigidly linked guanidinium groups in these complexes do not interact with the phosphodiester group undergoing cleavage but were able to enhance DNA binding by forming favorable interactions with neighboring phosphodiester groups within the sugar−phosphate backbone. As part of our continued efforts to develop more efficient synthetic nucleases through the combined use of metal ions and auxiliary functional groups, we now report the synthesis, characterization, and cleavage properties of the copper(II) complexes of three tacn ligands featuring single alkyl guanidine pendants (Figure 1, L^1−L^3). One of our goals was to maintain the enhanced reactivity of the *bis*(alkylguanidinium) complexes toward simple phosphodiester compounds, while reducing steric bulk to improve access of the Cu(II) center to the sugar−phosphate backbone of DNA with the expectation that nuclease activity could be enhanced. In addition to determining the crystal structures of the copper(II) complexes and the magnetic properties of the hydroxo-bridged complex formed by L^1, we have investigated the kinetics of cleavage of three phosphodiester-containing compounds, namely, BNPP, HPNPP, and pBR 322 plasmid DNA.

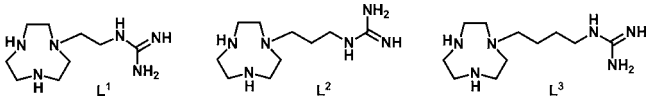

Figure 1. Ligands, L^1, L^2, and L^3, prepared in this study as tetrahydrochloride salts.

EXPERIMENTAL SECTION

Materials and Chemicals. Chemicals and solvents were of reagent or analytical grade and were used as received unless otherwise indicated. Distilled H_2O and high-performance liquid chromatography grade chloroform were used throughout. Tetrahydrofuran (THF) was dried over 4 Å molecular sieves and then freshly distilled from Na/benzophenone prior to use. 1,4-*bis*(*tert*-Butoxycarbonyl)-1,4,7-triazacyclononane[51] and sodium 2-hydroxypropyl-*p*-nitrophenylphosphate (NaHPNPP)[52,53] were synthesized according to literature procedures. The pBR 322 plasmid DNA was purchased from Promega Corporation. Milli-Q water used for DNA cleavage was sterilized by autoclaving, and all reaction solutions were prepared according to standard sterile techniques. Deoxygenated water was prepared by boiling distilled water under nitrogen for 4 h and cooling while bubbling with nitrogen gas. High-purity nitrogen gas was used directly from a reticulated system.

Instrumentation and Methods. Infrared spectra were recorded as KBr disks using a Bruker Equinox FTIR spectrometer at 4.0 cm^{-1} resolution, fitted with an ATR platform. Microanalyses were performed by Campbell Microanalytical Service (Otago, New Zealand). ^1H NMR and ^{13}C NMR spectra were recorded at 25 °C in D_2O or $CDCl_3$ (as listed) on a Bruker AC200, AM300, or DX400 spectrometer. Chemical shifts were recorded on the δ scale in parts per million (ppm) and were calibrated using either tetramethylsilane (TMS) or signals due to the residual protons of deuterated solvents. Abbreviations used to describe the resonances for ^1H NMR spectra are as follows: s (singlet), d (doublet), t (triplet), q (quartet), m (multiplet), and br s (broad singlet). Low-resolution electrospray ionization mass spectra (ESI-MS) were measured with a Micromass Platform II Quadrupole Mass Spectrometer fitted with an electrospray source. The capillary voltage was set at 3.5 eV, and the cone voltage at 35 V. Thin-layer chromatography (TLC) was performed using silica gel 60 F-254 (Merck) plates with detection of species present by UV irradiation or $KMnO_4$ oxidation. UV−vis-NIR spectra were recorded in 1 cm quartz cuvettes using Varian Cary Bio 300 or 5G spectrophotometers. Agarose gel electrophoresis of plasmid DNA cleavage products was performed using a Biorad Mini-Protean 3 Electrophoresis Module. Bands were visualized by UV light irradiation, fluorescence imaged using an AlphaImager, and photographed with a CCD camera. The gel photographs were analyzed with the aid of the program ImageQuaNT version 4.1.

Caution: Although no problems were encountered in this work, perchlorate salts are potentially explosive. They should be prepared in small quantities and handled with care.

Syntheses. *1-(2-Phthalimidoethyl)-4,7-bis(tert-butoxycarbonyl)-1,4,7-triazacyclononane (1).* A solution of 2-bromoethylphthalimide (0.370 g, 1.40 mmol) in CH_3CN (50 mL) was added dropwise to a mixture of 1,4-*bis*(*tert*-butoxycarbonyl)-1,4,7-triazacyclononane (0.470 g, 1.40 mmol), K_2CO_3 (0.470 g, 3.40 mmol), and KI (0.120 g, 0.600 mmol) in CH_3CN (50 mL), and the resulting mixture was stirred for 1 h at room temperature and then refluxed for 3 days. After it was cooled to room temperature, the inorganic salts were filtered off, and the solvent was removed under reduced pressure to yield **1** as a yellow oil. Yield: 0.47 g (65%). ^1H NMR (300 MHz, $CDCl_3$): δ 1.34 (s, 18H, ^{t}Bu CH_3), 2.74 (m, 6H, ethyl CH_2 and tacn CH_2), 3.15−3.37 (m, 8H, tacn CH_2), 3.65 (m, 2H, ethyl CH_2), 7.65 (m, 2H, aromatic CH), 7.85 (m, 2H, aromatic CH). ^{13}C NMR (75 MHz, $CDCl_3$): δ 28.2 (^{t}Bu CH_3), 35.7, 39.7 (ethyl CH_2), 47.8−53.7 (tacn CH_2), 79.2 (^{t}Bu quaternary C), 123.1, 131.8, 133.8 (aromatic CH), 155.3 (C=O), 168.0 (C=O). IR (neat), υ (cm^{-1}): 3473w (υ_{N-H}), 3058w ($\upsilon_{C-H(aromatic)}$), 2974s (υ_{C-H}), 1773s ($\upsilon_{C=O}$), 1682s ($\upsilon_{C=O}$), 1456s, 1393s, 1249s (υ_{C-O}), 1152s, 1018m, 986m, 868m, 773m, 720s, 620m. ESI-MS (m/z): 503.3 (90%) $[M + H]^+$, 525.2 (10%) $[M + Na]^+$.

dx.doi.org/10.1021/ic2019814 | *Inorg. Chem.* 2012, 51, 939−953

*1-(3-Phthalimidopropyl)-4,7-bis(tert-butoxycarbonyl)-1,4,7-triazacyclononane (**2**).* Compound **2** was prepared in an identical manner to **1** using 3-bromopropylphthalimide (0.450 g, 1.70 mmol), 1,4-*bis*(*tert*-butoxycarbonyl)-1,4,7-triazacyclononane (0.550 g, 1.70 mmol), K_2CO_3 (0.470 g, 3.40 mmol), and KI (0.120 g, 0.600 mmol) in CH_3CN (50 mL). The crude product was purified by column chromatography (Merck Silica Gel 60, eluent: CH_2Cl_2/diethyl ether, 7/3 v/v), with the desired fraction having an R_f = 0.71. Yield: 0.55 g (63%). ^{1}H NMR (300 MHz, $CDCl_3$): δ 1.43 (s, 18H, ^{t}Bu CH_3), 1.80 (m, 2H, ethyl CH_2), 2.54−2.67 (m, 6H, ethyl CH_2 and tacn ring CH_2), 3.29 (m, 4H, tacn ring CH_2), 3.45 (m, 4H, tacn ring CH_2), 3.75 (m, 2H, ethyl CH_2), 7.73 (m, 2H, aromatic CH), 7.85 (m, 2H, aromatic CH). ^{13}C NMR (75 MHz, $CDCl_3$): δ 27.1 (propyl CH_2), 28.5 (^{t}Bu CH_3), 36.3 (propyl CH_2), 49.3, 49.8, 50.2, 50.7, 53.8, 54.5 (tacn CH_2), 51.4 (propyl CH_2), 79.4 (^{t}Bu quaternary C), 123.1, 132.2, 133.8 (aromatic CH), 155.7 (C═O), 168.4 (C═O). IR (neat), υ (cm^{-1}): 3469w (υ_{N-H}), 3058w ($\upsilon_{C-H(aromatic)}$), 2973s (υ_{C-H}), 1770s ($\upsilon_{C=O}$), 1714s ($\upsilon_{C=O}$), 1455s, 1393s, 1250s (υ_{C-O}), 1150s, 1037s, 990m, 860m, 773m, 720s, 620m. ESI-MS (m/z): 517.2 (100%) $[M + H]^+$.

*1-(4-Phthalimidobutyl)-4,7-bis(tert-butoxycarbonyl)-1,4,7-triazacyclononane (**3**).* The synthesis was as for **1**. Yield: 65%. ^{1}H NMR (300 MHz, $CDCl_3$): δ 1.45 (s, 20H, ^{t}Bu CH_3 and butyl CH_2), 1.62−1.85 (m, 4H, butyl CH_2), 2.54−2.63 (m, 4H, tacn ring CH_2), 3.23 (m, 4H, tacn ring CH_2), 3.46 (m, 4H, tacn ring CH_2), 3.73 (m, 2H, butyl CH_2), 7.70 (m, 2H, aromatic CH), 7.85 (m, 2H, aromatic CH). ^{13}C NMR (75 MHz, $CDCl_3$): δ 26.3 (butyl CH_2), 28.5 (^{t}Bu CH_3), 30.5, 37.9, (butyl CH_2), 49.5, 49.7, 50.5, 50.9, 53.9, 54.0 (tacn CH_2), 56.1 (butyl CH_2), 79.3 (^{t}Bu quaternary C), 123.1, 132.2, 133.8 (aromatic CH), 155.7 (C═O), 168.4 (C═O). IR (neat), υ (cm^{-1}): 3470w (υ_{N-H}), 3058w ($\upsilon_{C-H(aromatic)}$), 2975s (υ_{C-H}), 2935s, 2865s, 1771s ($\upsilon_{C=O}$), 1714s ($\upsilon_{C=O}$), 1463s, 1398s, 1250s (υ_{C-O}), 1171s, 1045m, 990m, 861m, 774m, 734s, 647m. ESI-MS (m/z): 531.3 (100%) $[M + H]^+$.

*1-(2-Aminoethyl)-4,7-bis(tert-butoxycarbonyl)-1,4,7-triazacyclononane (**4**).* Hydrazine monohydrate (0.530 g, 10.0 mmol) was added to a solution of **1** (0.750 g, 1.50 mmol) in EtOH (50 mL), and the solution was heated at 50 °C for 4 h. After it was cooled to room temperature, the white precipitate that formed was removed by filtration, and the filtrate was evaporated to dryness to yield an oily residue, which was dissolved in CH_2Cl_2 (50 mL). After it was washed with 1 M NaOH (2 × 50 mL) and dried with Na_2SO_4, the solvent was removed under vacuum to yield **4** as a yellow oil. Yield: 0.45 g (80%). ^{1}H NMR (300 MHz, $CDCl_3$): δ 1.46 (s, 18H, ^{t}Bu CH_3), 1.62 (s br, 2H, NH_2), 2.63 (m, 8H, ethyl CH_2 and tacn CH_2), 3.25−3.47 (m, 8H, tacn CH_2). ^{13}C NMR (75 MHz, $CDCl_3$): δ 28.5 (^{t}Bu CH_3), 40.1, (ethyl CH_2), 48.7, 49.8, 50.8, 51.2, 53.9, 54.5 (tacn CH_2), 51.3 (ethyl CH_2), 79.6 (^{t}Bu quaternary C), 155.6 (C═O). IR (neat), υ (cm^{-1}): 3369w (υ_{N-H}), 2974s (υ_{C-H}), 2933s (υ_{C-H}), 1694s ($\upsilon_{C=O}$), 1463s, 1416s, 1366s, 1249s (υ_{C-O}), 1166s, 1100m, 990m, 860m, 773m. ESI-MS (m/z): 373.3 (100%) $[M + H]^+$.

*1-(3-Aminopropyl)-4,7-bis(tert-butoxycarbonyl)-1,4,7-triazacyclononane (**5**).* The synthesis was as for **4**. Yield: 73%. ^{1}H NMR (300 MHz, $CDCl_3$): δ 1.31 (s br, 2H, NH_2), 1.48 (s, 18H, ^{t}Bu CH_3), 1.52 (m, 2H, propyl CH_2), 2.49 (m, 2H, propyl CH_2), 2.58 (m, 4H, tacn CH_2), 2.68 (m, 2H, propyl CH_2), 3.22 (m, 4H, tacn CH_2), 3.41 (m, 4H, tacn CH_2). ^{13}C NMR (75 MHz, $CDCl_3$): δ 28.4 (^{t}Bu CH_3), 31.7, 40.2 (propyl CH_2) 49.3, 49.6, 50.4, 50.8, 53.6, 54.4 (tacn CH_2), 51.4 (propyl CH_2), 79.3 (^{t}Bu quaternary C), 155.5 (C═O). IR (neat), υ (cm^{-1}): 3371w (υ_{N-H}), 2975s (υ_{C-H}), 2933s (υ_{C-H}), 2861s (υ_{C-H}), 1690s ($\upsilon_{C=O}$), 1463s, 1414s, 1366s, 1249s (υ_{C-O}), 1174s, 1098s, 990s, 860m, 773m, 620m. ESI-MS (m/z): 387.2 (100%) $[M + H]^+$.

*1-(4-Aminobutyl)-4,7-bis(tert-butoxycarbonyl)-1,4,7-triazacyclononane (**6**).* The synthesis was as for **4**. Yield: 81%. ^{1}H NMR (300 MHz, $CDCl_3$): δ 1.31 (s br, 2H, NH_2), 1.45 (s, 22H, ^{t}Bu CH_3 and butyl CH_2), 2.47 (m, 2H, butyl CH_2), 2.67 (m, 6H, tacn CH_2 and butyl CH_2), 3.24 (m, 4H, tacn CH_2), 3.50 (m, 4H, tacn CH_2). ^{13}C NMR (75 MHz, $CDCl_3$): δ 25.3 (butyl CH_2), 28.5 (^{t}Bu CH_3), 31.5, 42.2 (butyl CH_2), 49.6, 49.8, 50.6, 51.1, 53.9, 54.1 (tacn CH_2), 56.6 (butyl CH_2), 79.4 (^{t}Bu quaternary C), 155.7 (C═O). IR (neat), υ (cm^{-1}): 3371w (υ_{N-H}), 2975s (υ_{C-H}), 2932s (υ_{C-H}), 1692s ($\upsilon_{C=O}$), 1463s, 1416s, 1366s, 1249s (υ_{C-O}), 1155s, 989m, 860m, 772m. ESI-MS (m/z): 401.4 (100%) $[M + H]^+$.

*1-{2-[bis(tert-Butoxycarbonyl)guanidino]ethyl}-4,7-bis(tert-butoxycarbonyl)-1,4,7-triazacyclononane (**7**).* To a stirred solution of **4** (0.490 g, 1.30 mmol) in THF (20 mL) was added *N*,*N*′-Boc$_2$-1*H*-pyrazole-1-carboxamidine (0.410 g, 1.30 mmol) dissolved in THF (20 mL). The resulting solution was stirred at room temperature for 2 days. The solvent was then removed under reduced pressure, and the residue was dissolved in CH_2Cl_2 (50 mL). After it was washed with 0.1 M NaOH (3 × 30 mL), the organic fraction was dried with Na_2SO_4, and the solvent was removed under reduced pressure to yield the crude product. Purification by column chromatography (Merck Silica Gel 60, eluent: 2% MeOH/$CHCl_3$) yielded the pure product as a pale yellow oil (R_f = 0.30). Yield: 0.54 g (67%). ^{1}H NMR (300 MHz, $CDCl_3$): δ 1.45 (s, 27H, ^{t}Bu CH_3), 1.49 (s, 9H, ^{t}Bu CH_3), 2.74 (m, 6H, tacn CH_2 and ethyl CH_2), 3.30 (m, 4H, tacn CH_2), 3.51 (m, 6H, tacn CH_2 and ethyl CH_2), 8.54 (t br, 1H, NH). ^{13}C NMR (75 MHz, $CDCl_3$): δ 28.0 (^{t}Bu CH_3), 28.2 (^{t}Bu CH_3), 28.5 (^{t}Bu CH_3), 39.4 (ethyl CH_2), 49.6, 50.6, 54.5, 55.2 (tacn CH_2), 56.2 (ethyl CH_2), 79.0, 79.3, 82.9 (^{t}Bu quaternary C), 126.0 (C═N), 155.5, 156.0, 163.5 (C═O). IR (neat), υ (cm^{-1}): 3334s (υ_{N-H}), 3131 m (υ_{N-H}), 2973s (υ_{C-H}), 1732s ($\upsilon_{C=O}$), 1662s ($\upsilon_{C=O}$), 1634s ($\upsilon_{C=O}$), 1557s ($\upsilon_{C=N}$), 1455s, 1249s (υ_{C-O}), 1156s, 1056s, 988s, 918s, 859s. ESI-MS (m/z): 615.3 (100%) $[M + H]^+$.

*1-{3-[bis(tert-Butoxycarbonyl)guanidino]propyl}-4,7-bis(tert-butoxycarbonyl)-1,4,7-triazacyclononane (**8**).* The synthesis was as for **7**, with purification by column chromatography (R_f = 0.35). Yield: 72%. ^{1}H NMR (300 MHz, $CDCl_3$): δ 1.47 (s, 27H, ^{t}Bu CH_3), 1.50 (s, 9H, ^{t}Bu CH_3), 1.62 (s br, 1H, NH), 1.73 (m, 2H, propyl CH_2), 2.56 (m, 2H, propyl CH_2), 2.65 (m, 4H, tacn CH_2), 3.28 (m, 4H, tacn CH_2), 3.46 (m, 6H, tacn CH_2 and propyl CH_2), 8.33 (t br, 1H, NH). ^{13}C NMR (75 MHz, $CDCl_3$): δ 27.6 (propyl CH_2), 27.9, 28.2, 28.4 (^{t}Bu CH_3), 38.8 (propyl CH_2), 49.3, 49.5, 50.4, 51.0, 53.8, 53.9 (tacn CH_2), 54.3 (propyl CH_2), 78.8, 79.2, 82.8 (^{t}Bu quaternary C), 153.1 (C═N), 155.4, 156.0, 163.5 (C═O). IR (neat), υ (cm^{-1}): 3334s (υ_{N-H}), 3138m (υ_{N-H}), 2921s (υ_{C-H}), 2950s (υ_{C-H}), 1732s ($\upsilon_{C=O}$), 1662s ($\upsilon_{C=O}$), 1614s ($\upsilon_{C=O}$), 1574s ($\upsilon_{C=N}$), 1470s, 1455s, 1249s (υ_{C-O}), 1047s, 991s, 918s, 858s, 731s. ESI-MS (m/z): 629.1 (90%) $[M + H]^+$, 651.1 (10%) $[M + Na]^+$.

*1-{4-[bis(tert-Butoxycarbonyl)guanidino]butyl}-4,7-bis(tert-butoxycarbonyl)-1,4,7-triazacyclononane (**9**).* The synthesis was as for **7**, with purification by column chromatography (R_f = 0.32). Yield: 71%. ^{1}H NMR (300 MHz, $CDCl_3$): δ 1.36 (s, 27H, ^{t}Bu CH_3), 1.39 (s, 11H, ^{t}Bu CH_3 and butyl CH_2), 1.55 (m, 2H, butyl CH_2), 2.41 (m, 2H, butyl CH_2), 2.52 (m, 4H, tacn CH_2), 3.16 (m, 4H, tacn CH_2), 3.36 (m, 6H, tacn CH_2 and butyl CH_2), 8.21 (t br, 1H, NH). ^{13}C NMR (75 MHz, $CDCl_3$): δ 24.9, 26.6 (butyl CH_2), 27.8, 28.1, 28.3 (^{t}Bu CH_3), 40.6 (butyl CH_2), 49.2, 49.5, 50.4, 51.0, 53.7, 54.0 (tacn CH_2), 56.1 (butyl CH_2), 78.9, 79.1, 82.7 (^{t}Bu quaternary C), 153.0 (C═N), 155.3, 155.9, 163.4 (C═O). IR (neat), υ (cm^{-1}): 3332s (υ_{N-H}), 3139m (υ_{N-H}), 2977s (υ_{C-H}), 2933s (υ_{C-H}), 1695s ($\upsilon_{C=O}$), 1681s ($\upsilon_{C=O}$), 1634s ($\upsilon_{C=O}$), 1555s ($\upsilon_{C=N}$), 1455s, 1252s (υ_{C-O}), 1157s, 1051s, 990s, 919s, 858s. ESI-MS (m/z): 643.2 (90%) $[M + H]^+$, 665.2 (10%) $[M + Na]^+$.

1-(2-Guanidinoethyl)-1,4,7-triazacyclononane Tetrahydrochloride (L^1·4HCl). Compound **7** (0.470 g, 0.770 mmol) was dissolved in a 1:1 (v/v) mixture of TFA and CH_2Cl_2 (10 mL), and the solution was stirred at room temperature overnight. The solvent was then removed under reduced pressure, and the resulting hygroscopic brown oil was dissolved in a mixture of EtOH (5 mL) and concentrated HCl (2 mL). The addition of diethyl ether (5 mL) produced a white precipitate, which was collected by filtration, dissolved in a small volume of water, and then freeze-dried to yield the product as a white solid. Yield: 0.12 g (71%). Microanalysis: calcd for $C_9H_{31}N_6Cl_4$: C, 27.3; H, 8.0; N, 21.3; Cl, 34.5%. Found: C, 27.3; H, 7.6; N, 21.2; Cl, 35.8%. ^{1}H NMR (300 MHz, D_2O): δ 3.06 (t, 2H, ethyl CH_2), 3.15 (m, 4H, tacn CH_2), 3.44 (m, 4H, tacn CH_2), 3.51 (t, 2H, J = 7.2 Hz, ethyl CH_2), 3.75 (s, 4H, tacn CH_2). ^{13}C NMR (75 MHz, D_2O): δ 37.8 (ethyl CH_2), 42.6, 44.3, 47.9 (tacn CH_2), 52.8 (ethyl CH_2), 157.2 (C═N). IR (KBr

dx.doi.org/10.1021/ic2019814 | *Inorg. Chem.* 2012, 51, 939−953

disk), υ (cm^{-1}): 3404s (υ_{N-H}), 2977s (υ_{C-H}), 2960s (υ_{C-H}), 1618s ($\upsilon_{C=N}$), 1450m, 1230w, 1178w, 940w. ESI-MS (m/z): 108.2 (90%) $[M + 2H]^{2+}$, 215.2 (10%) $[M + H]^{+}$.

1-(3-Guanidinopropyl)-1,4,7-triazacyclononane Tetrahydrochloride (L^2·4HCl). The synthesis was as for L^1·4HCl. Yield: 78%. Microanalysis: calcd for $C_{10}H_{32}N_6Cl_4$: C, 30.6; H, 7.8; N, 21.1; Cl, 33.2%. Found: C, 30.6; H, 7.6; N, 21.4; Cl, 33.8%. ^{1}H NMR (300 MHz, D_2O): δ 1.94 (m, 2H, propyl CH_2), 2.90 (m, 2H, propyl CH_2), 3.11 (m, 4H, tacn CH_2), 3.29 (t, 2H, J = 7.2 Hz, propyl CH_2), 3.44 (m, 4H, tacn CH_2), 3.69 (s, 4H, tacn CH_2). ^{13}C NMR (75 MHz, D_2O): δ 23.7, 39.5 (propyl CH_2), 42.3, 43.9, 47.6 (tacn CH_2), 52.2 (propyl CH_2), 157.1 (C═N). IR (KBr disk), υ (cm^{-1}): 3412s (υ_{N-H}), 2954s (υ_{C-H}), 1610s ($\upsilon_{C=N}$), 1436m, 1172w, 1018w. ESI-MS (m/z): 115.2 (90%) $[M + 2H]^{2+}$, 229.2 (10%) $[M + H]^{+}$.

1-(4-Guanidinobutyl)-1,4,7-triazacyclononane Tetrahydrochloride (L^3·4HCl). The synthesis was as for L^1·4HCl. Yield: 72%. Microanalysis: calcd for $C_{11}H_{35}N_6Cl_4$: C, 30.3; H, 7.7; N, 19.0; Cl, 34.3%. Found: C, 30.5; H, 8.1; N, 19.4; Cl, 32.8%. ^{1}H NMR (300 MHz, D_2O): δ 1.68 (m, 4H, butyl CH_2), 2.94 (m, butyl CH_2), 3.24 (m, 6H, tacn CH_2 and butyl CH_2), 3.41 (m, 4H, tacn CH_2), 3.60 (s, 4H, tacn CH_2). ^{13}C NMR (75 MHz, D_2O): δ 21.5, 26.0, 41.2 (butyl CH_2), 42.2, 43.2, 48.0 (tacn CH_2), 55.2 (butyl CH_2), 157.1 (C═N). IR (KBr disk), υ (cm^{-1}): 3378s (υ_{N-H}), 2977s (υ_{C-H}), 2788s (υ_{C-H}), 1608s ($\upsilon_{C=N}$), 1503s, 1256w, 1160w, 968w. ESI-MS (m/z): 243.3 (100%) $[M + H]^{+}$.

*$[Cu_2L^1{}_2(\mu\text{–}OH)](ClO_4)_3\cdot H_2O$ (**C1**).* To a stirred aqueous solution (4 mL) of L^1·4HCl (0.097 g, 0.250 mmol) was added $Cu(ClO_4)_2\cdot 6H_2O$ (0.120 g, 0.290 mmol) dissolved in water (4 mL). The pH of solution was adjusted to 9 with the addition of 1 M NaOH, resulting in a color change to a darker blue and the precipitation of a small amount of $Cu(OH)_2$, which was removed by filtration. The deep blue solution was left to slowly evaporate in a crystallizing dish, eventually yielding dark blue crystals of **C1**. Yield: 75 mg (34%). Microanalysis: calcd for $Cu_2C_{18}H_{47}N_{12}O_{14}Cl_3$: C, 24.3; H, 5.3; N, 18.9%. Found: C, 24.3; H, 5.2; N, 18.6%. UV–vis (H_2O): λ_{max} (nm) [ε_{max}] (M^{-1} cm^{-1}): 626 [113], 987 [36]. IR bands (ATR) υ (cm^{-1}): 3446m (υ_{O-H}), 3378m, 3242m, 3306m (υ_{N-H}), 2984w, 2884w (υ_{C-H}), 1615s ($\upsilon_{C=N}$), 1464m, 1359m, 1274w, 1065s br, 621s (υ_{ClO4^-}).

*$[Cu(L^2H)Cl_2]Cl\cdot(MeOH)_{0.5}\cdot(H_2O)_{0.5}$ (**C2**).* An aqueous solution (4 mL) of L^2·4HCl (0.097 g, 0.230 mmol) was added to $Cu(ClO_4)_2\cdot 6H_2O$ (0.130 g, 0.280 mmol) dissolved in water (4 mL). The adjustment of the pH to 9 with 1 M NaOH, followed by removal of $Cu(OH)_2$ by filtration, gave a deep blue solution, which was evaporated to dryness. The residue was dissolved in MeOH, and the product was crystallized by diffusion of diethyl ether into this solution. Yield: 35 mg (36%). Microanalysis: calcd for $CuC_{10.5}H_{28}N_6OCl_3$: C, 29.7; H, 6.7; N, 19.8%. Found: C, 29.6; H, 6.4; N, 20.1%. UV–vis (H_2O): λ_{max} (nm) [ε_{max}] (M^{-1} cm^{-1}): 618 [91], 957 [29]. IR bands (ATR) υ (cm^{-1}): 3246m, 3149m (υ_{N-H}), 2941w, 2874w (υ_{C-H}), 1652s ($\upsilon_{C=N}$), 1450m, 1375w, 1280w, 1095w, 1023w, 954w, 888w, 830w.

*$[Cu(L^3H)Cl_2]Cl\cdot(DMF)_{0.5}\cdot(H_2O)_{0.5}$ (**C3**).* The synthesis was as for **C2**, except that L^3·4HCl (0.100 g, 0.240 mmol) and $Cu(ClO_4)_2\cdot 6H_2O$ (0.150 g, 0.280 mmol) were used. The product was crystallized by dissolving the residue in *N*,*N*′-dimethylformamide and diffusing diethyl ether into this solution. Yield: 38 mg (35%). Microanalysis: calcd for $CuC_{12.5}H_{31.5}N_{6.5}OCl_3$: C, 32.7; H, 6.9; N, 19.8%. Found: C, 32.6; H, 6.8; N, 20.2%. UV–vis (H_2O): λ_{max} (nm) [ε_{max}] (M^{-1} cm^{-1}): 620 [103], 948 [35]. IR bands (ATR) υ (cm^{-1}): 3320m, 3262m, 3124m, (υ_{N-H}), 2931w, 2862w (υ_{C-H}), 1625s ($\upsilon_{C=N}$), 1492m, 1257w, 1161w, 1039w, 960w, 869w, 757w, 633w.

Derivation of Protonation and Dimerization Constants. Equilibrium constants for protonation and dimerization reactions of **C1**–**C3** were derived from systematic series of spectra collected (400–1300 nm) at varying pH (~4–12) and complex concentrations (5–15 mM). The series of spectra were analyzed using the BEEROZ software.[54] Briefly, this method employs constraints from mass balance and mass action equations to test the speciation models for spectral data sets containing many species and to derive formation constants for the spectroscopically active species.[55,56] The analysis provides the calculated spectra based on the model, the spectra for the individual complexes, and formation constants for all of the species included in the model. For the present study, activity coefficients were fixed to unity (fixed ionic strength).

Cleavage of Model Phosphate Esters. *BNPP.* These experiments were conducted using established procedures.[57,58] Briefly, the cleavage of BNPP by the Cu(II) complexes was measured at pH 7.0 (HEPES) and 9.0 (CHES) at T = 50 °C, by following the formation of *p*-nitrophenoxide ion (λ_{max} = 400 nm, ε_{max} = 18700 M^{-1} cm^{-1}) in solutions containing 0.1 mM BNPP, 2 mM Cu(II) complex, and 0.15 M $NaClO_4$. Absorbance measurements were commenced 2 min after mixing and were continued for 8000 min, with a reading taken every 5 min. As the complex was in large excess as compared to BNPP, the time dependence of the appearance of NP (and cleavage of BNPP) was modeled as a first-order process, and observed rate constants (k_{obs}) were determined by fitting the data to the equation, Abs = $A + Be^{-k_{obs}t}$, where A and B are constants.

HPNPP. These experiments were carried out in a similar manner to the BNPP experiments. The cleavage of HPNPP by the Cu(II) complexes was measured at pH 6.0 (MES), 7.0 (HEPES), and 9.0 (CHES) at T = 25 °C by following the release of the *p*-nitrophenoxide ion in solutions containing 0.1 mM HPNPP, 2 mM Cu(II) complex, and 0.15 M $NaClO_4$, and k_{obs} was determined as for the BNPP cleavage studies.

DNA Cleavage Experiments. These experiments also followed established procedures.[49,50] Reaction mixtures (total volume = 15 μL) containing supercoiled pBR 322 plasmid DNA (38 μM base pair concentration) and copper(II) complexes (75, 100, 150, 225, 300, 450, and 600 μM) in 40 mM buffers (MES, HEPES, TAPS, and CHES) at pH 6.0, 6.5, 7.0, 7.5, 8.0, 8.5, and 9.0 were incubated in a water bath at 37 °C for periods of up to 48 h. The loading buffer was added to stop the reactions at defined time periods, and the resulting solutions were stored at −20 °C until just prior to analysis. The resulting solutions were loaded onto 1% agarose gels containing 1.0 μg dm^{-3} ethidium bromide. The DNA fragments were separated by gel electrophoresis [70 V for 2 h in 1 × Tris-acetate EDTA (TAE) buffer]. Ethidium-stained agarose gels were imaged, and the extent of supercoiled DNA cleavage was determined via densitometric analysis of the visualized bands using the volume quantification method. In all cases, background fluorescence was determined by reference to a lane containing no DNA. Supercoiled pBR 322 DNA intensity values were multiplied by 1.42 to account for the increased ability of ethidium bromide to intercalate into supercoiled DNA (form I) as compared to nicked DNA (form II).[26,49,50] The DNA cleavage data were fitted to a first-order expression, % DNA = $A + Be^{-k_{obs}t}$, yielding the first-order rate constant, k_{obs}, for cleavage of form I DNA to produce form II.

DNA Cleavage Experiments in the Presence of Radical Scavengers. Aliquots (5 μL) of aqueous solutions of scavenging agents (30 mM KI, DMSO, ^{t}BuOH, or NaN_3 in 40 mM HEPES buffer at pH 7.0) were added to the solutions of supercoiled DNA (5 μL, 113.5 μM base pair concentration) prior to the addition of complexes **C1**, **C2**, and **C3**. The final reaction conditions were: [complex] = 150 μM, [scavenging agents] = 10 mM, and [DNA] = 38 μM base pair concentration. Each solution was incubated at 37 °C for 6 h, quenched, and analyzed according the procedures described above.

DNA Cleavage under Anaerobic Conditions. Experiments under anaerobic condition were performed following the protocol reported by Burstyn and co-workers[6] and in our previous work.[49,50] All other conditions were as for the cleavage experiments performed under aerobic conditions in which final concentrations for the reaction mixtures were 150 μM for complexes, 40 mM HEPES buffer, and 38 μM base pair concentration for supercoiled DNA.

X-ray Crystallography. Intensity data for blue crystals of **C1** (0.20 × 0.10 × 0.05 mm^3), **C2** (0.18 × 0.15 × 0.05 mm^3), and **C3** (0.15 × 0.12 × 0.05 mm^3) were collected at 123 K on a Bruker Apex II CCD fitted with graphite monochromated Mo Kα radiation (0.71073 Å). The data were collected to a maximum 2θ value of 55° (50° for C1, the high angle data was dominated by noise [$I/\sigma(I)$ < 1.0] and was omitted) and processed using Bruker Apex II software package. Crystal

dx.doi.org/10.1021/ic2019814 | Inorg. Chem. 2012, 51, 939–953

Scheme 1. Synthesis of Hydrochloride Salts of Ligands L^1, L^2, and L^3[a]

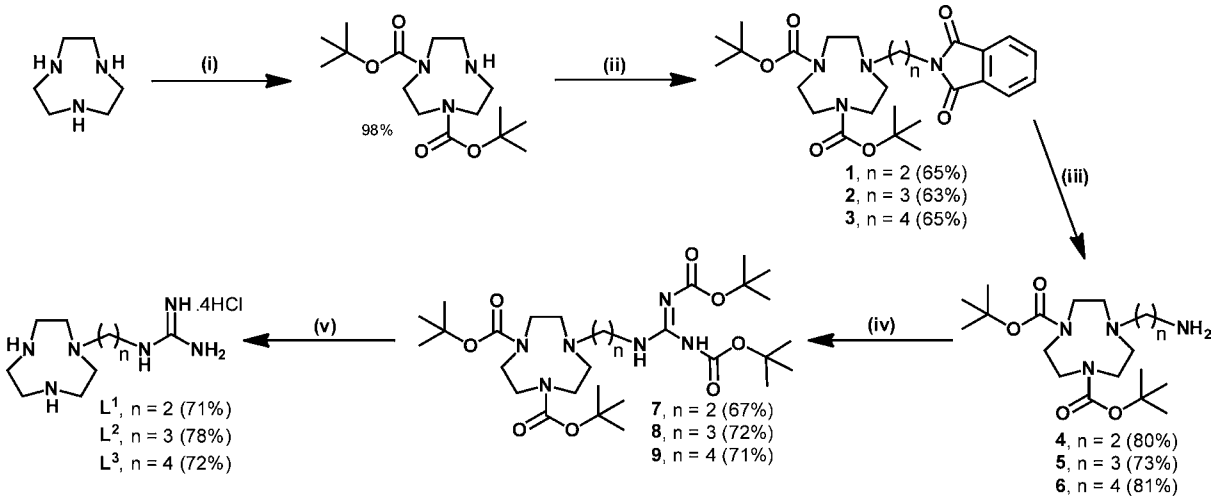

[a]Reagents and conditions: (i) 2 equiv of Boc-ON, NEt_3, $CHCl_3$, RT, 8 h. (ii) Bromoalkylphthalimide, K_2CO_3, KI, CH_3CN, reflux, 3 days. (iii) $N_2H_4{\cdot}H_2O$, EtOH, 50 °C, 4 h. (iv) *N,N′*-Boc_2-1*H*-pyrazole-1-carboxamidine, THF, RT, 2 days. (v) (a) TFA/CH_2Cl_2 (1:1), RT, o/n; (b) concentrated HCl.

parameters and details of the data collection are summarized in Table S01 in the Supporting Information.

The structures of **C1**, **C2**, and **C3** were solved using SHELX-97[59,60] and expanded using standard Fourier transform routines. All hydrogen atoms were placed in idealized positions, except for the hydrogen atoms on the nitrogen atoms, which were located on the Fourier difference map. All nonhydrogen atoms were refined anisotropically.

RESULTS AND DISCUSSION

Preparation of Ligands and Complexes. Scheme 1 describes in detail the route employed to prepare the new guanidine-bearing derivatives of tacn from the di-Boc-protected tacn precursor (Boc_2tacn).[51] Each of compounds **1**–**9** and L^1–$L^3{\cdot}$4HCl were obtained in reasonable to high yields (60–80%), and the identity of each was established by ^1H and ^{13}C NMR spectroscopy and ESI-MS. The ^{13}C NMR spectra of **7**–**9** exhibited signals at ca. 163.5 and 156.0 ppm, which were assigned to the carbonyl type carbons of the Boc_2-guanidine group. A signal at ca. 153 ppm, assigned to the C═N moiety of the guanidine group, further suggested that **7**–**9** had been formed. This signal shifted to 157 ppm for the final ligands.

The copper(II) complexes of L^1–L^3, $[Cu_2L^1_2(\mu\text{–OH})](ClO_4)_3$ (**C1**), $[Cu(L^2H)Cl_2]Cl{\cdot}(MeOH)_{0.5}{\cdot}(H_2O)_{0.5}$ (**C2**), and $[Cu(L^3H)Cl_2]Cl{\cdot}(DMF)_{0.5}{\cdot}(H_2O)_{0.5}$ (**C3**) were prepared as described in the Experimental Section. The microanalyses were consistent with these formula, and the IR spectra showed NH vibrations in the 3240–3380 cm^{-1} region and sharp υ(C═N) vibrations at ca. 1620 cm^{-1} attributable to the guanidine pendant groups. Complex **C1** also showed a broad OH vibration centered at 3446 cm^{-1} and typical perchlorate vibrations. The electronic spectra of **C1**–**C3** measured in water exhibited bands at ca. 620 and 950–990 nm, typical for square pyramidal (SP) copper(II) complexes.[61]

Crystallography. *$[Cu_2L^1_2(\mu\text{-OH})](ClO_4)_3{\cdot}H_2O$ (**C1**).* X-ray structural analysis revealed that **C1** has two Cu(II) centers linked by a single μ-hydroxo bridge (Figure 2). Only half of the molecule resides in the asymmetric unit (ASU), while the other half was generated by crystallographic symmetry about the μ-hydroxo bridge. The two copper atoms are at a distance of 3.655(3) Å, making a nonlinear Cu–O–Cu angle of 139.8(2)° about the hydroxo bridge vertex. Comparison of the Cu–OH–

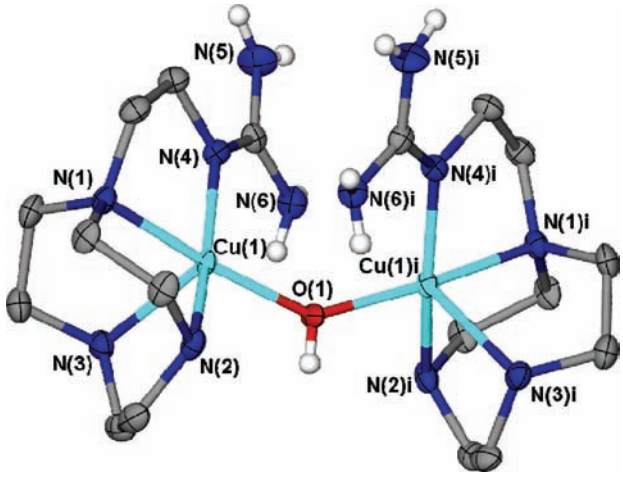

Figure 2. Thermal ellipsoid plot of the complex cation in **C1** (ellipsoids drawn at 50% probability). Atoms denoted i are generated by symmetry (2 − *x*, *y*, 1/2 − *z*).

Cu core in **C1** with other $[Cu_2(\mu\text{-OH})_2]^{2+}$ or $[Cu_2(\mu\text{-OH})]^{3+}$ cores indicates that the Cu–O distance lies within the usual range [1.900(4)–2.019(3) Å] observed for such cores (Table 1). However, in comparison to the di-μ-hydroxo-bridged complexes, a larger separation between the two Cu(II) centers in **C1** is an obvious outcome of the Cu–O–Cu angle being more obtuse in the former (Table 1) and of the absence of a second bridging hydroxo group. A similar Cu–O–Cu angle of 135.2(3)° has previously been reported for an imidazole pendant-bearing Cu(II)–tacn complex, $[Cu_2L^{im}_2(\mu\text{-OH})]^{3+}$, where the two metal centers were also connected by a monohydroxo bridge.

The copper geometry in **C1** is distorted SP. The τ value of 17%, calculated using the method described by Addison et al.,[62] indicates a slight degree of distortion from the ideal SP geometry (τ = 0%) toward trigonal bipyramidal (TBP) geometry (τ = 100%). As expected, the Cu(1)–N(3) distance for the apical nitrogen atom [2.246(3) Å] is slightly longer than the Cu–N(1) and N(2) bond lengths [2.032(3) Å and

dx.doi.org/10.1021/ic2019814 | *Inorg. Chem.* 2012, 51, 939–953

Table 1. Structural Data for Mono- and Di-μ-hydroxo-Bridged Cu(II)-tacn Complexes

complex[a]	Cu−O (Å)	Cu−O−Cu (deg)	refs
C1	1.946(1)	139.8(2)	this work
$[Cu_2L^{im}_2(\mu\text{-}OH)]^{3+}$	1.913(4); 1.925(5)	135.2(3)	63
$[Cu_3L^{mes}(\mu\text{-}OH)_2(H_2O)_2](ClO_4)_4{\cdot}2H_2O$	1.900(4); 2.019(3)	98.9(2)	64
	1.922(3); 2.015(3)	92.1(1)	
$[Cu_6(L^{mes})_2(\mu\text{-}OH)_6](ClO_4)_6{\cdot}2H_2O$	1.957(3); 1.920(4)	94.7(1)	64
	1.954(3); 1.919(4)	97.0(1)	
	1.933(4); 1.969(4)	98.7(2)	
$[Cu_2(Me_3tacn)_2(\mu\text{-}OH)_2](ClO_4)_2$	1.939(4); 1.936(4)	100.1(2)	65
$[Cu_2(\mu\text{-}OH)(\mu\text{-}CH_3COO)(tacn)_2(\mu\text{-}H_2O)]^{2+}$	1.963(2)	114.3(2)	66
$[Cu_2L^{mx}(\mu\text{-}OH)_2](BPh_4)_2$	1.928(2); 1.931(2)	99.6(1)	67
$[Cu_4L^{dur}(\mu\text{-}OH)_4](ClO_4)_4$	1.961(8); 1.975(8)	97.9(4)	68
	1.936(7); 1.989(9)	95.7(4)	
$[Cu_2(Butacn)_2(\mu\text{-}OH)_2](ClO_4)_2$	1.929(2)	101.01(9)	69
$[Cu_2(Fc^iPr_2tacn)_2(\mu\text{-}OH)_2](ClO_4)_2$	1.960(7); 1.946(7)	101.1(3)	70
$[Cu_2(Bn_3tacn)(Bn_2tacn)(\mu\text{-}OH)_2](CF_3SO_3)_2{\cdot}2(^iPrOH)$	1.949(4); 1.924(5)	100.5(2);100.5(8)	71
$[Cu_2(^iPr_2tacn)_2(\mu\text{-}OH)_2](BPh_4)_2{\cdot}2THF$	1.922(6); 1.951(6)	100.9(3);102.7(3)	71
$[Cu_2(Bn^iPr_2)_2(\mu\text{-}OH)_2](CF_3SO_3)_2$	1.950(6); 1.933(6)	101.1(3);102.9(3)	71
$[Cu_2(\mu\text{-}OH)_2(Me_2tacn)_2](ClO_4)_2$	1.941(3); 1.952(3)	97.9(1);97.9(1)	58
$[Cu_2(\mu_2\text{-}OH)_2(BnMe_2tacn)_2](ClO_4){\cdot}H_2O$	1.926 (3); 1.944 (3)	97.0(1);96.0(1)	58
$[Cu_2(\mu_2\text{-}OH)_2$ (cyanoBn$_3$tacn)$_2](ClO_4)_2{\cdot}2H_2O$	1.944(3); 1.945(3)	95.8(1);96.1(1)	58

[a]Abbreviations: L^{im}, 1-(1-methylimidazol-2-ylmethyl)-1,4,7-triazacyclononane; L^{mes}, 1,3,5-*tris*(1,4,7-triazacyclonon-1-ylmethyl)benzene; Me_3tacn, 1,4,7-trimethyl-1,4,7-triazacyclononane; L^{mx}, 1,3-*bis*(1,4,7-triazacyclonon-1-ylmethyl)benzene; L^{dur}, 1,2,4,5-tetrakis(1,4,7-triazacyclonon-1-ylmethyl)-benzene; Butacn, *N*-4-(but-1-ene)-1,4,7-triazacyclononane; Fc^iPr_2tacn, 1-ferrocenylmethyl-4,7-diisopropyl-1,4,7-triazacyclononane; Bn_3tacn, 1,4,7-tribenzyl-1,4,7-triazacyclononane; Bn_2tacn, 1,4-dibenzyl-1,4,7-triazacyclononane; $^iPr_2tacn$, 1,4-diisopropyl-1,4,7-triazacyclononane; Bn^iPr_2tacn, 1-benzyl-4,7-diisopropyl-1,4,7-triazacyclononane; Me_2tacn, 1,4-dimethyl-1,4,7-triazacyclononane; $BnMe_2tacn$, 1-benzyl-4,7-dimethyl-1,4,7-triazacyclononane; and cyanoBn_3tacn, 1,4,7-*tris*(3-cyanobenzyl)-1,4,7-triazacyclononane.

2.038(3) Å, respectively] that form the part of the basal plane (Table 2). The oxygen atom, O(1), of the μ-hydroxo group and

Table 2. Selected Bond Lengths (Å) and Angles (°) for C1[a]

Cu(1)−O(1)	1.946(1)	O(1)−Cu(1)−N(4)	98.7(1)
Cu(1)−N(1)	2.032(3)	O(1)−Cu(1)−N(1)	170.7(9)
Cu(1)−N(2)	2.038(3)	N(4)−Cu(1)−N(1)	82.8(1)
Cu(1)−N(3)	2.246(3)	O(1)−Cu(1)−N(2)	91.6(1)
Cu(1)−N(4)	1.996(3)	N(4)−Cu(1)−N(2)	160.5(1)
		N(1)−Cu(1)−N(2)	84.4(1)
		O(1)−Cu(1)−N(3)	105.6(1)
		N(4)−Cu(1)−N(3)	110.5(1)
		N(1)−Cu(1)−N(3)	82.3(1)
		N(2)−Cu(1)−N(3)	82.3(1)
		Cu(1)#2−O(1)−Cu(1)	139.8(2)

[a]Symmetry transformations used to generate equivalent atoms: #1, $-x + 1, y, -z + 1/2$; #2, $-x + 2, y, -z + 1/2$.

the nitrogen atom, N(4), from the guanidine pendant complete the basal plane, with Cu(1)−O(1) and Cu(1)−N(4) bond distances of 1.946(1) and 1.996(3) Å, respectively. This type of guanidine coordination mode was previously observed for the Cu(II) complex of 1-ethyl-4,7-*bis*(ethylguanidine)-1,4,7-triaza-cyclononane.[49] As in our previous study, the high affinity of the guanidine in L^1 for copper(II) is highlighted by the fact that the Cu−N distance is shorter than those involving the macrocyclic nitrogens, viz. 1.996(3) vs 2.032(3)−2.246(3) Å.[49]

A least-squares analysis of the basal planes formed by atoms N(1)/N(4)/O(1)/N(2) and their symmetry equivalents reveals a dihedral angle of 61.75°, with the two guanidinium pendants pointing away from each other (Figure 3). This may be to minimize the steric and electrostatic repulsion between these pendant and their symmetry equivalents (symmetry

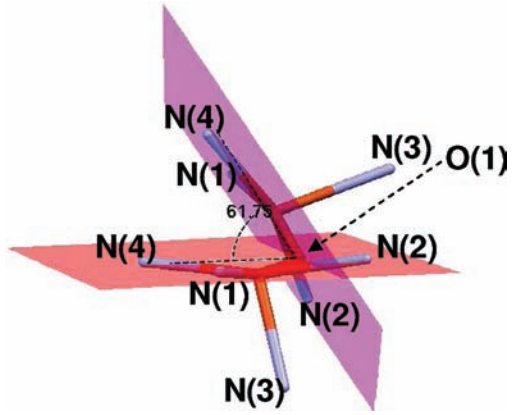

Figure 3. Relative orientation of the two Cu(II) SP coordination polyhedra in **C1** with the dihedral angle between the least-squares basal planes indicated.

operation: $2 - x, y, 1/2 - z$). The guanidine groups are themselves skewed relative to each other (angle of 26.6° between their least-squares planes) and further held in their respective positions by hydrogen bonding with an oxygen atom from the perchlorate anion present in the crystal lattice (Figure S01 in the Supporting Information and Table 3).

*$[Cu(L^2H)Cl_2]Cl{\cdot}(MeOH)_{0.5}{\cdot}(H_2O)_{0.5}$ (**C2**).* The crystal structure of **C2** shows that the ASU contains two complex units, distinguished within the crystal lattice by their relative distances from a co-crystallized methanol molecule (Figure 4). The two molecules are connected in a head-to-tail arrangement, due to an intermolecular hydrogen-bonding interaction between them [N(6)−H(6AN)···Cl(3): 3.262(2) Å, 162(2)°].

The Cu(II) centers are five-coordinate and exhibit distorted SP geometry, with τ = 10 and 13% for Cu(1) and Cu(2),

dx.doi.org/10.1021/ic2019814 | *Inorg. Chem.* 2012, 51, 939−953

Table 3. Hydrogen-Bonding Interactions in C1 (Å and °)[a]

D−H···A	d(D−H)	d(H···A)	d(D···A)	∠(DHA)
N(2)−H(2)···O(2)#3	0.87(1)	2.19(1)	3.062(4)	179(4)
N(3)−H(3)···O(3)#4	0.87(1)	2.33(1)	3.190(5)	168(3)
N(5)−H(5C)···O(5)	0.87(1)	2.19(3)	2.976(5)	149(4)
N(5)−H(5D)···O(6)#2	0.88(1)	2.32(2)	3.158(5)	160(3)
N(6)−H(6D)···O(7)#5	0.88(1)	2.32(2)	3.177(4)	165(4)
N(6)−H(6C)···O(1)	0.88(1)	2.36(3)	2.925(4)	122(3)

[a]Symmetry transformations used to generate equivalent atoms: #1, $-x+1, y, -z+1/2$; #2, $-x+2, y, -z+1/2$; #3, $x-1/2, y-1/2, -z+1/2$; #4, $-x+5/2, y-1/2, z$; and #5, $x+1, y, z$.

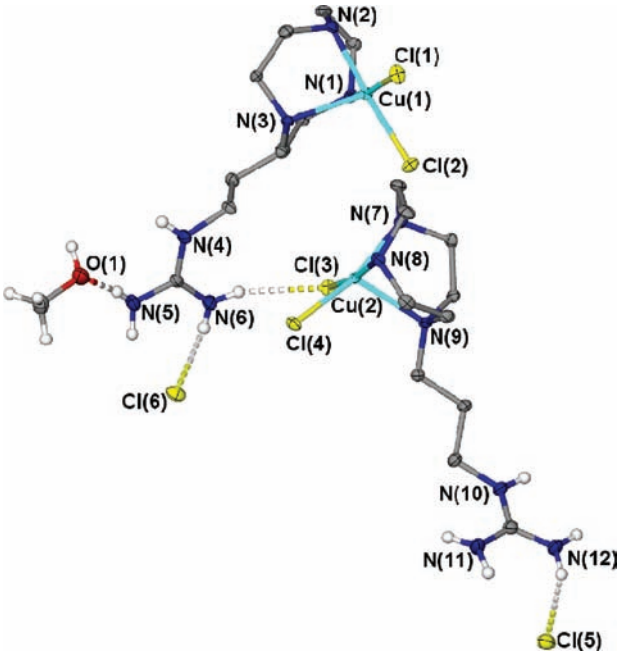

Figure 4. Thermal ellipsoid plot of the asymmetric unit of **C2** showing noncoordinating chloride anions and methanol molecule (ellipsoids drawn at 50% probability; selected hydrogen atoms are omitted for clarity; dashed bonds indicate intermolecular hydrogen-bonding interactions).

respectively. The base of the pyramid is defined by the two Cl atoms, and the two secondary nitrogens [N(1)/N(2)/Cl(1)/Cl(2) and N(7)/N(8)/Cl(4)/Cl(3) for Cu(1) and Cu(2), respectively], while the apical site is occupied by the macrocyclic nitrogen atom bearing the propyl guanidinium pendant. The two sets of basal atoms have a mean deviation of 0.069 and 0.074 Å, respectively, from their least-squares planes, with the two copper atoms, Cu(1) and Cu(2), lying out of the plane by 0.20 and 0.19 Å, respectively.

The basal Cu−Cl distances, for example, Cu(1)−Cl(1) = 2.2758(5) Å and Cu(1)−Cl(2) = 2.2941(6) Å, are typical for such coordinate bonds.[61] In both molecular units, the Cu−N axial distance is elongated with respect to the Cu−N basal distances by >0.20 Å (Table 4), as is typical for d^9 Cu(II) centers with a SP geometry.[72] The bond angles around the Cu(II) center are typical for Cu(II)−tacn derivatives.[73−75]

In both molecular units, the propylguanidinium pendant is protonated, with the pendant extending away from the metal center and forming hydrogen-bonding interactions with the chloro ligands (Figure S02 in the Supporting Information and Table 5). As mentioned before, within the ASU, the coordinated chloride ligand, Cl(3), connects the two cationic

Table 4. Selected Bond Lengths (Å) and Angles (°) for C2

Cu(1)−N(1)	2.020(2)	N(1)−Cu(1)−N(2)	83.07(7)
Cu(1)−N(2)	2.038(2)	N(1)−Cu(1)−N(3)	83.17(6)
Cu(1)−N(3)	2.275(2)	N(2)−Cu(1)−N(3)	82.22(7)
Cu(1)−Cl(1)	2.2758(5)	N(1)−Cu(1)−Cl(1)	164.83(5)
Cu(1)−Cl(2)	2.2941(6)	N(2)−Cu(1)−Cl(1)	90.94(5)
Cu(2)−N(8)	2.020(2)	N(3)−Cu(1)−Cl(1)	109.90(4)
Cu(2)−N(7)	2.039(2)	N(1)−Cu(1)−Cl(2)	90.15(6)
Cu(2)−N(9)	2.265(2)	N(2)−Cu(1)−Cl(2)	170.92(5)
Cu(2)−Cl(4)	2.2855(5)	N(3)−Cu(1)−Cl(2)	103.05(4)
Cu(2)−Cl(3)	2.2922(5)	Cl(1)−Cu(1)−Cl(2)	94.13(2)
		N(8)−Cu(2)−N(7)	82.96(7)
		N(8)−Cu(2)−N(9)	82.50(7)
		N(7)−Cu(2)−N(9)	83.39(6)
		N(8)−Cu(2)−Cl(4)	88.82(5)
		N(7)−Cu(2)−Cl(4)	164.14(5)
		N(9)−Cu(2)−Cl(4)	109.04(4)
		N(8)−Cu(2)−Cl(3)	171.96(5)
		N(7)−Cu(2)−Cl(3)	91.04(5)
		N(9)−Cu(2)−Cl(3)	102.19(4)
		Cl(4)−Cu(2)−Cl(3)	95.70(2)

Table 5. Hydrogen-Bonding Interactions in C2 (Å and °)[a]

D−H···A	d(D−H)	d(H···A)	d(D···A)	∠(DHA)
N(5)−H(5BN)···O(1)	0.80(3)	2.12(3)	2.900(3)	166(3)
N(5)−H(5AN)···Cl(6)#1	0.86(2)	2.50(2)	3.221(2)	141(2)
N(6)−H(6AN)···Cl(3)	0.84(2)	2.45(2)	3.262(2)	162(2)
N(6)−H(6BN)···Cl(6)	0.80(3)	2.45(3)	3.230(2)	168(2)
O(1)−H(1O)···Cl(5)#2	0.84	2.34	3.070(2)	146.2
N(4)−H(4N)···Cl(5)#2	0.77(2)	2.50(2)	3.269(2)	175(2)
N(12)−H(13N)···Cl(5)	0.84(3)	2.41(3)	3.205(2)	157(2)
N(10)−H(10N)···Cl(6)#3	0.87(2)	2.39(2)	3.212(2)	158(2)
N(12)−H(12N)···Cl(6)#3	0.90(2)	2.38(2)	3.212(2)	154(2)
N(1)−H(1N)···Cl(1)#4	0.76(2)	2.57(2)	3.234(2)	147(2)
N(8)−H(8N)···Cl(3)#5	0.75(2)	2.59(2)	3.270(2)	152(2)
N(11)−H(11N)···Cl(5)	0.90(3)	2.51(3)	3.342(2)	154(2)

[a]Symmetry transformations used to generate equivalent atoms: #1, $-x+1, -y+1, -z+2$; #2, $x-1, -y+1/2, z-1/2$; #3, $-x+1, y-1/2, -z+5/2$; #4, $x, -y+1/2, z+1/2$; and #5, $x, -y+1/2, z-1/2$.

units in a head-to-tail fashion via hydrogen bonding. This hydrogen-bonding network is extended in the third dimension by the cocrystallized methanol molecule and chloride anions present in the lattice. The chloride counteranions, Cl(6) and Cl(5), serially link the protonated guanidine pendants in the crystal lattice to each other by means of hydrogen bonds (Table 5). This network is further extended by hydrogen bonding with the methanol molecule, which acts as hydrogen bond acceptor to the guanidine protons and donor to the chloride anions.

*$[Cu(L^3H)Cl_2]Cl\cdot(DMF)_{0.5}\cdot(H_2O)_{0.5}$ (**C3**).* As for **C2**, the Cu(II) center in **C3** lies in a distorted SP geometry (Figure 5), τ value of 9%, comprised of three facially coordinating nitrogen atoms from tacn and two chloride ligands. The secondary nitrogens, N(1) and N(2), along with Cl(1) and Cl(2), define the basal plane with the deviation from the least-squares plane being 0.042 Å. The tertiary nitrogen atom with the butylguanidinium pendant attached forms the apex of the pyramid. The two Cu−Cl basal distances and other bond angles and bond lengths are within the expected ranges (Table 6).[61,72,75] The deviation of the copper center from the least-squares basal plane toward the apical nitrogen N(3) is 0.25 Å, which is slightly larger than in **C2**.

dx.doi.org/10.1021/ic2019814 | Inorg. Chem. 2012, 51, 939−953

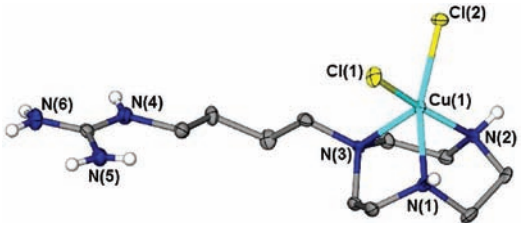

Figure 5. Thermal ellipsoid representation of **C3** (ellipsoids drawn at 50% probability; hydrogen atoms on carbon and counteranions have been omitted for clarity).

Table 6. Selected Bond Lengths (Å) and Angles (°) for C3

Cu(1)−N(1)	2.034(4)	N(2)−Cu(1)−N(1)	83.3(2)
Cu(1)−N(2)	2.021(3)	N(2)−Cu(1)−N(3)	83.5(1)
Cu(1)−N(3)	2.254(4)	N(1)−Cu(1)−N(3)	82.2(2)
Cu(1)−Cl(1)	2.264(1)	N(1)−Cu(1)−Cl(1)	92.0(1)
Cu(1)−Cl(2)	2.314(1)	N(2)−Cu(1)−Cl(1)	168.3(1)
		N(3)−Cu(1)−Cl(1)	106.5(1)
		N(1)−Cu(1)−Cl(2)	163.1(1)
		N(2)−Cu(1)−Cl(2)	88.7(1)
		N(3)−Cu(1)−Cl(2)	111.71(4)
		Cl(1)−Cu(1)−Cl(2)	93.01(2)

Similar to **C2**, the nitrogen atom N(4) on the charged guanidinium pendant in **C3** is not coordinated. The terminal nitrogen on the guanidinium pendant forms charge-assisted hydrogen bonds with one chloro ligand, which further forms Cl···H−N hydrogen-bonding interactions with the secondary amine nitrogen on the macrocycle [N(6)−H(6AN)···Cl(3): 3.242(4) Å, 153(4)°; N(5)−H(5BN)···Cl(3): 3.181(5) Å, 159(4)°; N(1)−H(1N)···Cl(3)#1: 3.202(4) Å, 148(4)°, #1 denoting the symmetry operator $(-x + 3/2, y, z - 1/2)$]. This creates a chloro ligand-mediated 1D-helical chain with the molecules aligned in a head-to-tail arrangement in the crystal lattice (Figure S03 in the Supporting Information and Table 7).

Table 7. Hydrogen-Bonding Interactions in C3 (Å and °)[a]

D−H···A	*d*(D−H)	*d*(H···A)	*d*(D···A)	∠(DHA)
N(1)−H(1N)···Cl(3)#1	0.83(5)	2.47(5)	3.202(4)	148(4)
N(2)−H(2N)···Cl(1)#2	0.860(19)	2.54(3)	3.339(3)	154(4)
N(6)−H(6AN)···Cl(3)	0.858(19)	2.45(3)	3.242(4)	153(4)
N(5)−H(5BN)···Cl(3)	0.90(5)	2.33(5)	3.181(5)	159(4)

[a]Symmetry transformations used to generate equivalent atoms: #1, $-x + 3/2, y, z - 1/2$; and #2, $x - 1/2, -y + 1, z$.

Magnetic Properties of C1. Molar magnetic susceptibilities for **C1** were measured in a field of 1 T over the temperature range of 30−300 K. The variable temperature magnetic moment plot (see Figure 6) shows a decrease in magnetic moment with temperature, which is indicative of strong antiferromagnetic coupling between the copper(II) centers, mediated by the OH bridge. The 300 K value of 1.32 μ_B, per Cu(II), decreases with decreasing temperature and reaches a value of ca. 0.5 μ_B at ca. 100 K, after which the magnetic moment remains reasonably constant, the corresponding susceptibilities (Figure 6) showing Curie-like behavior. The increase in susceptibility observed between 100 and 30 K is most likely due to the presence of a monomeric "impurity", which is a commonly observed in Cu(II) complexes possessing antiferromagnetic interactions between the metal

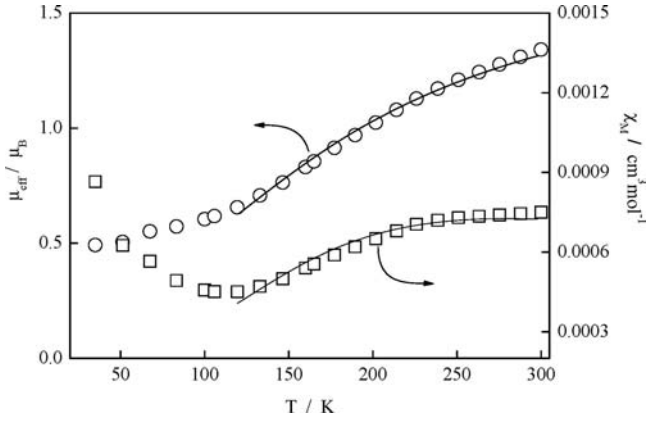

Figure 6. Plot of μ_{eff} and χ_M (per Cu) vs temperature for complex **C1**. The solid lines were calculated using the parameter set given in the text and are restricted to the 100−300 K region since this is the region sensitive to *J*.

centers.[76] The data were fitted to the modified Bleaney−Bowers[77] given in eq 1, yielding the following parameters: g = 2.01, J = −165 cm^{-1}, and P (fraction of S = 1/2 monomer) = 0.04, with a temperature-independent paramagnetism (Nα) per Cu(II) of 64 × 10^{-6} cm^3 mol^{-1}. This large, negative value of J is primarily due to strong antiferromagnetic coupling across the Cu−O(H)−Cu bridge and is compatible with the Cu−O−Cu bridge angle of 139.8(2)° and Cu···Cu separation of 3.655(3) Å. While di-μ-hydroxo bridging is most common in Cu(II) dimers, there is a small but growing number of singly OH-bridged examples, and the present example fits nicely into the magnetostructural correlations deduced from O(H) p-orbital bridging between Cu($d_{x^2-y^2}$) orbitals arising from SP Cu centers.[78]

$$\chi_{Cu} = \frac{Ng^2\beta^2}{kT}\left[3 + \exp\left(\frac{-2J}{kT}\right)\right]^{-1}(1 - P) + \frac{Ng^2\beta^2P}{4kT} + N\alpha \quad (1)$$

Aqueous Speciation. The results of the speciation calculations based on systematic variations in the UV−vis spectra are shown in Figure 7. Equilibrium constants for the preferred models are listed in Table 8. For **C1**, principal component analysis (PCA) suggests that a minimum of five species are required to explain the individual data sets at fixed concentration of **C1**. In practice, four species (as per speciation scheme in Figure 8) provided a good fit to the data: the χ^2 value corresponding to the absolute minimum was 3.25, and Δ_{abs} (largest difference between measured and calculated absorbances) was 0.025 units. Because a binuclear complex crystallizes from solutions of **C1**, we hypothesized that this complex might also be important in solution. Consequently, we investigated the effect of $[L^1{}_2Cu_2(OH)]^{3+}$ on the overall fit. The preferred model (Figure 7) (χ^2 = 4.46; Δ_{abs} = 0.028) is within the 90% confidence range of the fit corresponding to the absolute minimum[54,79] and shows the maximum amount of the binuclear complex among the fits within the 90% confidence level relative to the absolute minimum.

For **C2**, PCA clearly indicates that a minimum of five species are required to explain the UV−vis data set; this corresponds to the number of complexes in the simplified speciation model in Figure 9. The best-fit results using this model, shown in Figure

dx.doi.org/10.1021/ic2019814 | *Inorg. Chem.* 2012, 51, 939−953

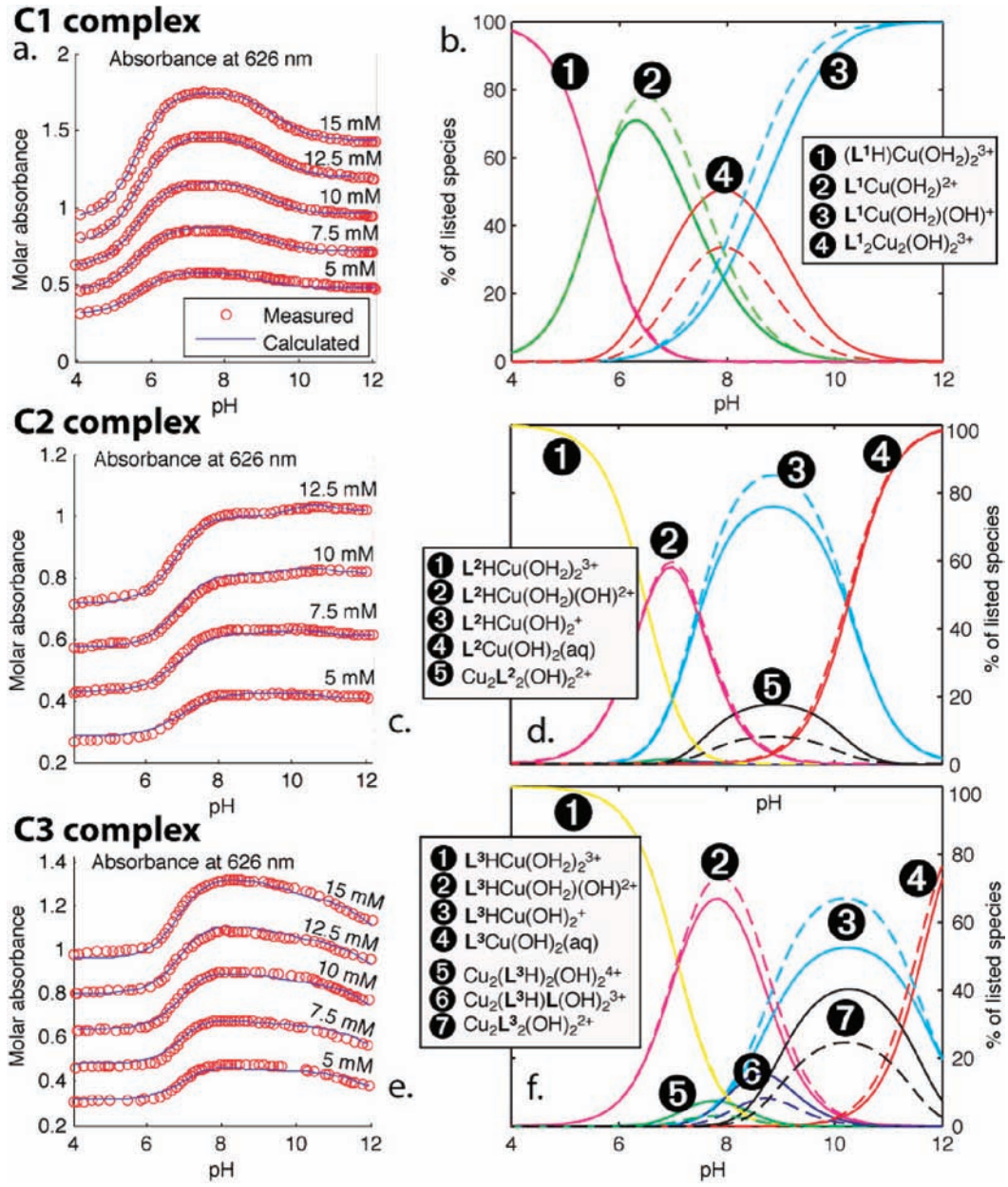

Figure 7. Results of UV−vis titrations and quantitative spectral analysis for **C1**, **C2**, and **C3**. (a, c, e) Absorbance data at a fixed wavelength of 626 nm, as a function of pH (*x*-axis) and total complex concentration. Circles are measurements; lines were calculated using the speciation model. (b, d, f) Distribution of species calculated from the quantitative analysis, calculated for complex concentrations of 5 (dashed lines) and 15 (plain lines) mM; corresponding stability constants are shown in Table 8.

7c,d (χ^2 = 1.26; Δ_{abs} = 0.028), indicate that the amounts of polynuclear species formed in this system are small.

For **C3**, PCA reveals that a minimum of six species are required to explain the UV−vis spectra. Our preferred model (Figure 7f) contains seven species (based on the speciation scheme in Figure 9), but the spectra of the minor binuclear complexes, $[Cu_2(L^3H)_2(OH)_2]^{4+}$ and $[Cu_2(L^3H)L^3(OH)_2]^{3+}$, were constrained to be equal during the fitting. As with the other systems, the similarity in the spectra of the individual complexes (Figure 7) results in some degrees of correlation between the formation constants of some complexes. The χ^2 value corresponding to the absolute minimum was 1.81 (Δ_{abs} = 0.067). For **C3**, the concentration of polynuclear complexes was highly sensitive of the log K_D value; the favored solution has a χ^2 value of 2.07 (Δ_{abs} = 0.070), which is within the 90% confidence level for the solution corresponding to the absolute minimum.[54,79] This solution was preferred because it displays the most reasonable spectra for the individual complexes (Figure S04 in the Supporting Information). We note, in particular, that in many fits the molar absorbance for $[Cu_2L^2(OH)_2]^{2+}$ was similar to those of the mononuclear species, suggesting that the amount of polynuclear species at pH ≥ 9 was overestimated. From the favored solution, it can be inferred that <10% of species present at pH ≤ 8 are polynuclear (Figure 7f).

Within the limits of measurement and fitting of spectrophotometric data, the concentration of binuclear complexes present at the concentrations used is concluded to be low for **C2** and **C3**. As will be discussed further below, it then follows that under the conditions of the kinetic experiments ([complex] of

dx.doi.org/10.1021/ic2019814 | *Inorg. Chem.* 2012, 51, 939−953

Table 8. Proposed Protonation and Dimerization Constants for C1−C3

$(L^1H)Cu(H_2O)_2^{3+} = L^1Cu(H_2O)^{2+} + H^+ + H_2O$	$pK_{a1} = 5.6$
$L^1Cu(H_2O)^{2+} = L^1Cu(OH)^+ + H^+$	$pK_{a2} = 7.9$
$L^1Cu(H_2O)^{2+} + L^1Cu(OH)^+ = L^1{}_2Cu_2(HO)^{3+} + H_2O$	Log $K_d = 2.9$
$L^2HCu(H_2O)_2^{3+} = L^2HCu(H_2O)(OH)^{2+} + H^+$	$pK_{a1} = 6.5$
$L^2HCu(H_2O)(OH)^{2+} = L^2HCu(OH)_2^+ + H^+$	$pK_{a2} = 7.5$
$L^2HCu(OH)_2^+ = L^2Cu(OH)_2 + H^+$	$pK_{a3} = 10$
$2L^2Cu(OH)(OH_2)^+ = L^2{}_2Cu_2(OH)_2^{2+} + 2H_2O$	Log $K_d = 1.4$
$L^3HCu(H_2O)_2^{3+} = L^3HCu(H_2O)(OH)^{2+} + H^+$	$pK_{a1} = 7.0$
$L^3HCu(H_2O)(OH)^{2+} = L^3HCu(OH)_2^+ + H^+$	$pK_{a2} = 8.9$
$L^3HCu(OH)_2^+ = L^3Cu(OH)_2 + H^+$	$pK_{a3} = 11.2$
$2L^3Cu(OH)(OH_2)^+ = L^3{}_2Cu_2(OH)_2^{2+} + 2H_2O$	Log $K_d = 2.3$
$2L^3HCu(H_2O)(OH)^{2+} = (L^3H)_2Cu_2(OH)_2^{4+} + 2H_2O$	Log $K_d = 0.7$
$(L^3H)_2Cu_2(OH)_2^{4+} = (L^3H)L^3Cu_2(OH)_2^{3+} + H^+$	Log $K_d = 6.7$

2 mM for BNPP/HPNPP cleavage and 75−600 μM for DNA cleavage), the concentration of binuclear complexes is even smaller, such that they are unlikely to affect the rates of cleavage.

Cleavage of Model Phosphate Esters. The rate constants for the cleavage of the model phosphodiesters, BNPP and HPNPP, measured in the presence of **C1**−**C3** at different pH values are summarized in Tables 9 and 10, together with data for related complexes. At all pH values and for both substrates, the three complexes enhanced the rate of cleavage well above background levels, particularly for the less reactive DNA mimic, BNPP (HPNPP, like RNA, features a 2′-OH group on the ribose ring that acts as an internal nucleophile). In addition, the reaction rate increased with pH, consistent with the proposed hydrolytic mechanism for Cu(II)−tacn-based complexes, which features a Cu(II)-bound hydroxide nucleophile as the active species.[1] {For simplicity, in the discussion of cleavage studies that follows, we refer to the parent complexes, **C1**−**C3**, but it should be emphasized that on dissolution, complicated equilibria will be established as elucidated from the speciation studies.}

The slowest rates of cleavage were measured for complex **C1**, which displayed similar reactivity to $[Cu(tacn)(OH_2)_2]^{2+}$. On the basis of the crystal structure and the results of speciation studies, which correspond well to the complex bearing two ethylguanidine pendants[49] above pH 6, **C1** exists in three major forms, $[Cu(L^1)(OH_2)]^{2+}$, $[Cu(L^1)(OH)]^+$, and the dimer, $[Cu_2(L^1)_2(\mu\text{-}OH)]^{3+}$ (Figure 7). Since for $[Cu(L^1)(OH)]^+$ and $[Cu_2(L^1)_2(\mu\text{-}OH)]^{3+}$ the Cu(II) coordination sphere is comprised of four nitrogen donor from the ligand and an oxygen from a hydroxo ligand, coordination of the substrate would require displacement of the hydroxo ligand, which is bound more strongly than the aqua ligand in $[Cu(L^1)(OH_2)]^{2+}$. Furthermore, even if binding occurs, no internal nucleophile (Cu−OH) is available to carry out the cleavage.[57,81] **C1** can therefore be considered to be surprisingly reactive. The rates of cleavage are slower than for $[Cu(tacn)(OH_2)_2]^{2+}$ but much faster than those of the Cu(II) complex of the ligand with two ethylguanidine pendants, $[Cu(\mathbf{A})]^{2+}$, whose Cu(II) coordination sphere is saturated by the ligand donor atoms.[49] For HPNPP, the reaction rates are similar to those for $[Cu(tacn)(OH_2)_2]^{2+}$, except at pH 6, where the rate of cleavage is faster for **C1**. At pH 6, about 50% of the complex exists as $[(L^1H)Cu(H_2O)_2]^{3+}$ and has a protonated guanidine pendant that may assist the cleavage of HPNPP through hydrogen-bonding/electrostatic interactions.

At pH 7, the rates of cleavage of BNPP and HNPP by **C2** and **C3** were faster than for **C1** (5−10-fold) and $[Cu(tacn)(OH_2)_2]^{2+}$ (3−5-fold), whereas at pH 9, the fastest rates were observed for **C3**, the most active complex in the series. **C3** is also more active than complexes with more rigid xylyl-linked guanidinium groups, $[Cu(\mathbf{C})(OH_2)_2]^{2+}$, $[Cu(\mathbf{D})(OH_2)_2]^{2+}$, and $[Cu(\mathbf{E})(OH_2)_2]^{2+}$.[50] The guanidinium groups in **C2** and **C3** appear to play an active role in cleavage. Assuming that cleavage involves mono aqua-hydroxo species, as proposed by Burstyn and co-workers,[1] the charged pendants may be enhancing substrate binding and stabilizing transition states through electrostatic/hydrogen-bonding interactions. That the

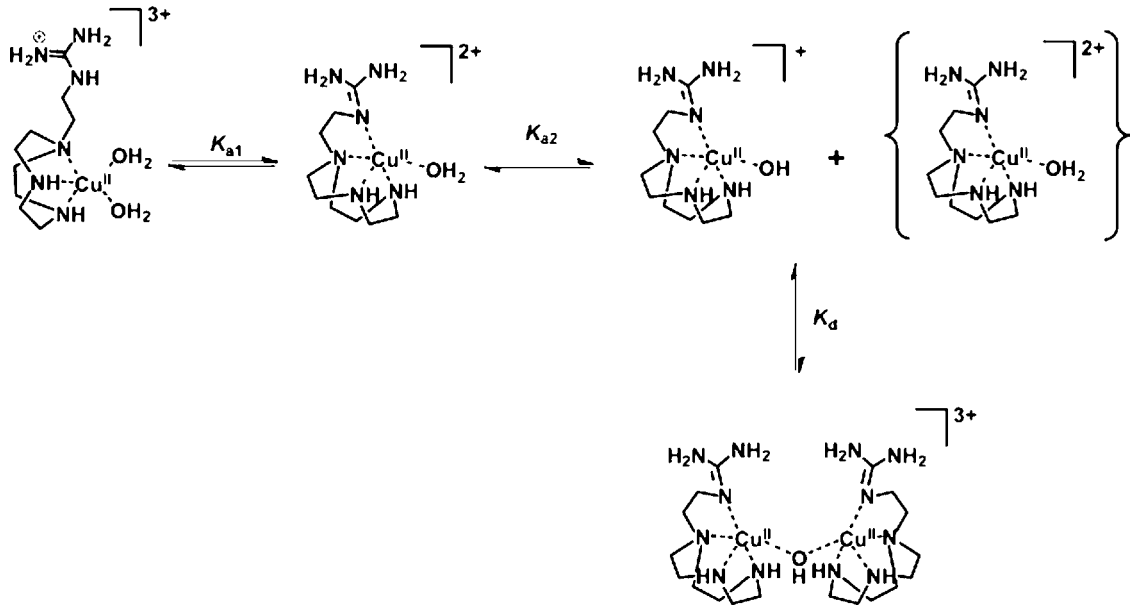

Figure 8. Proposed protonation and dimerization equilibria for complex **C1**.

dx.doi.org/10.1021/ic2019814 | *Inorg. Chem.* 2012, 51, 939−953

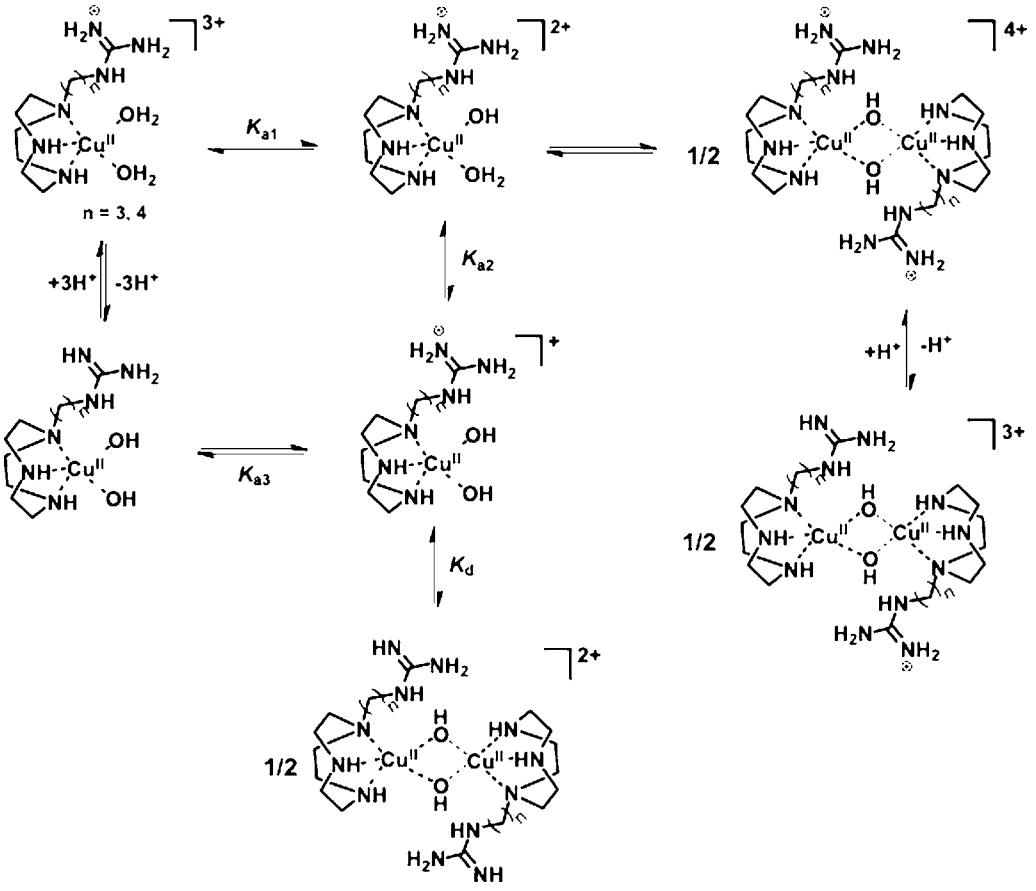

Figure 9. Proposed protonation and dimerization equilibria for complexes **C2** and **C3**.

guanidinium pendants contribute to activity is supported by the fact that addition of a second propylguanidinium pendant to **C2** leads to further increases in the rate of BNPP and HPNPP cleavage (cf. **C2** vs $[Cu(B)(OH_2)_2]^{2+}$ in Tables 9 and 10). It should be noted, however, that the cleavage rates for **C2** and **C3** fall within the range observed for di- and trialkylated tacn–copper(II) complexes.[57,58,75,80]

Cleavage of Plasmid DNA. The cleavage of pBR 322 plasmid DNA by complexes **C1**–**C3** was studied as function of pH and complex concentration, under aerobic and anaerobic conditions, and in the presence of radical scavengers. The results of these experiments are summarized in Figures 10–12 and S05–S26 in the Supporting Information and Tables 11 and S02–S12 in the Supporting Information. Incubation of pBR 322 plasmid DNA with complexes **C1**, **C2**, and **C3** converts the supercoiled form (form I) to the singly nicked relaxed from (form II) and to the double-nicked linear form (form III) toward the end of the 48 h incubation period (Figure 10). The rate of cleavage was 5–15-fold faster than for nonfunctionalized $[Cu(tacn)(OH_2)_2]^{2+}$ complex (see Table 11). For example, incubation of pBR 322 plasmid DNA for 6 h at pH 7.0 in the presence of 150 μM **C1**–**C3** converted 72–90% of the initial DNA to form II, cf., 20% for $[Cu(tacn)(OH_2)_2]^{2+}$. Control experiments confirmed that no measurable DNA cleavage occurred when pBR 322 plasmid DNA was incubated with a 150 μM concentration of either the nonmetalated ligands or $CuCl_2$ (see Figure S26 in the Supporting Information). This indicates that the species active in DNA cleavage are (or are derived from) complexes **C1**–**C3**. A predominantly hydrolytic (as opposed to redox-mediated) mode of cleavage was confirmed through experiments performed in the presence of various scavengers for reactive oxygen species (Figures S16–S21 in the Supporting Information), as well as under anaerobic conditions (Figures S22–S24 in the Supporting Information), consistent with earlier observations for related Cu(II)–tacn-based complexes.[6,49,50]

The propyl derivative, **C2**, exhibited the highest rate of DNA cleavage, being ca. 15 times more active than the Cu(II)–tacn complex and accelerating cleavage by a factor of 2×10^7 relative to the background rate.[82] The varying rates of DNA cleavage by the guanidine-bearing compounds indicate that DNA hydrolysis may be driven by cooperativity between the Cu(II) center and positively charged guanidinium group and that the degree of cooperativity can be favorably altered by tuning the length and nature of the pendant.[50] Complexes **C1**–**C3** are all more reactive than the analogues bearing two alkylguanidine pendants, $[Cu(\mathbf{A})]^{2+}$ and $[Cu(\mathbf{B})(OH_2)_2]^{2+}$, indicating that their reduced steric bulk probably allows better access of the Cu(II) center to the sugar–phosphate backbone. In the case of $[Cu(\mathbf{A})]^{2+}$, strong binding of the two guanidine pendants saturates the primary coordination sphere and also contributes to the reduced reactivity of this complex.

The enhanced rate of DNA cleavage by **C1**, when compared to BNPP, is consistent with our previous results on phosphate ester cleavage by the Cu(II)-*bis*-guanidinium tacn family,[49] where it was postulated that, on introduction of DNA, phosphodiester–guanidinium and phosphodiester–Cu(II) interactions induce detachment and protonation of the coordinated guanidines, leading to improved potency. For **C1**, this would create a vacant site on the Cu(II) center for an

dx.doi.org/10.1021/ic2019814 | *Inorg. Chem.* 2012, 51, 939–953

Table 9. First-Order Rate Constants for Hydrolysis of BNPP by Copper(II) tacn-Based Complexes[a]

compd	10^6 k_{obs} (s^{-1}) pH 7.0	pH 9.0	refs
control	0.0003		this work
$[Cu(tacn)(OH_2)_2]^{2+}$	1.71 ± 0.01	6.3	57
$[Cu_2L^1_2(\mu\text{-}OH)]^{3+}$ (**C1**)	1.35 ± 0.09	7.9 ± 0.5	this work
$[Cu(L^2)(OH_2)_2]^{2+}$ (**C2**)	7.0 ± 0.1	8.5 ± 0.5	this work
$[Cu(L^3)(OH_2)_2]^{2+}$ (**C3**)	10.2 ± 0.9	19 ± 3	this work
$[Cu(\mathbf{A})]^{2+}$[b]	0.0100 ± 0.0003	NR[d]	49
$[Cu(\mathbf{B})(OH_2)_2]^{2+}$	72.4 ± 0.8	63.5 ± 0.2	49
$[Cu(\mathbf{C})(OH_2)_2]^{2+}$	1.65 ± 0.03	3.07 ± 0.08	50
$[Cu(\mathbf{D})(OH_2)_2]^{2+}$	2.36 ± 0.03	7.02 ± 0.07	50
$[Cu(\mathbf{E})(OH_2)_2]^{2+}$	2.39 ± 0.04	7.49 ± 0.05	50
$[Cu(Me_2tacn)(OH_2)]^{2+}$[c]	12.4		58
$[Cu(Me_3tacn)(OH_2)]^{2+}$[c]	37		57
$[Cu(^iPr_3tacn)(OH_2)]^{2+}$[c]	43		80
$[Cu(Et^iPrtacn)(OH_2)]^{2+}$[c]	14.3		75
$[Cu(PrNH_2Bn^iPrtacn)(OH_2)]^{2+}$[c]	0.48 ± 0.001		75
$[Cu(Bn^iPrtacn)(OH_2)]^{2+}$[c]	15.3		75
$[Cu(BnMe_2tacn)(OH_2)]^{2+}$[c]	70.1		58

[a]Conditions used: [complex] = 2 mM, [BNPP] = 0.1 mM, [HEPES] = 50 mM, I = 0.15 M, and T = 50 °C. Solutions were prepared by dissolving samples of complexes **C1**−**C3**. Abbreviations: **A**, 1-ethyl-4,7-*bis*(2-guanidinoethyl)-1,4,7-triazacyclononane; **B**, 1-ethyl-4,7-*bis*(3-guanidinopropyl)-1,4,7-triazacyclononane; **C**, 1-(*o*-guanidinoxylyl)-1,4,7-triazacyclononane; **D**, 1-(*m*-guanidinoxylyl)-1,4,7-triazacyclononane; **E**, 1-(*p*-guanidinoxylyl)-1,4,7-triazacyclononane; Me_2tacn, 1,4-dimethyl-1,4,7-triazacyclononane; Me_3tacn, 1,4,7-trimethyl-1,4,7-triazacyclononane; $^iPr_3$tacn, 1,4,7-triisopropyl-1,4,7-triazacyclononane; Et^{i}Prtacn, 1-ethyl-4-isopropyl-1,4,7-triazacyclononane; Bn^{i}Prtacn, 1-benzyl-4-isopropyl-1,4,7-triazacyclononane; $BnMe_2$tacn, 1-benzyl-4,7-dimethyl-1,4,7-triazacyclononane [b]Data were analyzed using initial rate method, yielding k_{obs} indirectly, which was further converted to a first-order rate constant. [c]Aquo complexes formed on dissolution in aqueous solution. [dd] [d]NR, no reaction.

incoming phosphodiester on the DNA substrate to bind and activate.

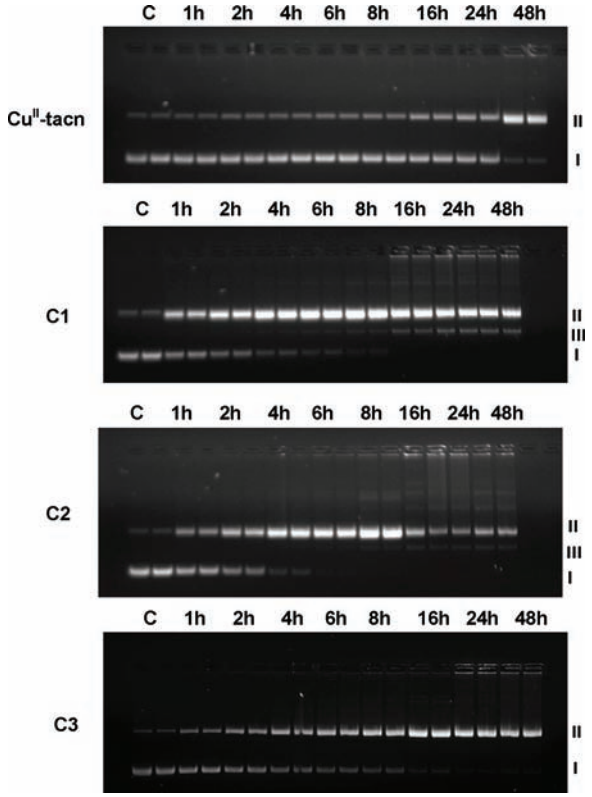

Figure 10. Agarose gel showing cleavage of pBR 322 plasmid DNA (38 μM bp) by $[Cu(tacn)(OH_2)_2]^{2+}$ and **C1**−**C3** (150 μM) in HEPES buffer (40 mM, pH 7.2) at 37 °C for various time intervals. Lanes 1 and 2, DNA control; lanes 3 and 4, 1 h; lanes 5 and 6, 2 h; lanes 7 and 8, 4 h; lanes 9 and 10, 6 h; lanes 11 and 12, 8 h; lanes 13 and 14, 16 h; lanes 15 and 16, 24 h; and lanes 17 and 18, 48 h.

The extent of plasmid DNA cleavage by complexes **C1**−**C3** was found to vary with pH and complex concentration in a very similar fashion to that previously observed for the *bis*(alkylguanidine)[49] and xylylguanidine complex series.[50] The plots of percentage cleavage versus [complex] and pH display a bell-like profile (Figures 11 and 12), with an optimal rate of DNA cleavage at a pH and [complex] of 7.0 and 150 μM, respectively, similar to those reported previously for synthetic nucleases.[57,58,75,80]

Table 10. First-Order Rate Constants for Cleavage of HPNPP by Copper(II) tacn-Based Complexes[a]

compd	10^6 k_{obs} (s^{-1}) pH 6.0	pH 7.0	pH 9.0	refs
HPNPP[b] only	0.019	0.012 ± 0.007	0.81	this work
$[Cu(tacn)(OH_2)_2]^{2+}$	~0.4[b]	3.6 ± 0.2[b]	8.7 ± 1.0	50
$[Cu_2L^1_2(\mu\text{-}OH)]^{3+}$ (**C1**)	1.16 ± 0.02	1.46 ± 0.09	7.53 ± 0.01	this work
$[Cu(L^2)(OH_2)_2]^{2+}$ (**C2**)	1.83 ± 0.02	14 ± 2	22.8 ± 0.3	this work
$[Cu(L^3)(OH_2)_2]^{2+}$ (**C3**)	2.77 ± 0.03	14.1 ± 0.7	45.7 ± 1.0	this work
$[Cu(\mathbf{A})]^{2+}$		0.13 ± 0.06		49
$[Cu(\mathbf{B})(OH_2)_2]^{2+}$		32 ± 3		49
$[Cu(\mathbf{C})(OH_2)_2]^{2+}$	0.754 ± 0.007	1.88 ± 0.03	3.27 ± 0.09	50
$[Cu(\mathbf{D})(OH_2)_2]^{2+}$	1.51 ± 0.02	2.74 ± 0.02	10.1 ± 0.6	50
$[Cu(\mathbf{E})(OH_2)_2]^{2+}$	0.936 ± 0.006	2.30 ± 0.03	9.55 ± 0.01	50

[a]Conditions used: [complex] = 2 mM, [HPNPP] = 0.1 mM, [HEPES] = 50 mM, I = 0.15 M, and T = 25 °C. Solutions were prepared by dissolving samples of complexes **C1**−**C3**. For abbreviations, see the footnotes to Table 9. [b]Data were analyzed using initial rate method, yielding k_{obs} directly. Value at pH 6 has been corrected using the effective molar extinction coefficient.

dx.doi.org/10.1021/ic2019814 | *Inorg. Chem.* 2012, 51, 939−953

Table 11. First-Order Rate Constants for Single-Strand Cleavage of pBR 322 Plasmid DNA by Copper(II) tacn-Based Complexes[a]

compd	$10^5\ k_{obs}$ (s^{-1})	refs
$[Cu(tacn)(OH_2)_2]^{2+}$	1.23 ± 0.37	49
$[Cu_2L^1{}_2(\mu\text{–}OH)]^{3+}$ (**C1**)	13.03 ± 0.13	this work
$[Cu(L^2)(OH_2)_2]^{2+}$ (**C2**)	18.73 ± 0.19	this work
$[Cu(L^3)(OH_2)_2]^{2+}$ (**C3**)	5.51 ± 0.03	this work
$[Cu(\mathbf{A})]^{2+}$	1.58 ± 0.05	49
$[Cu(\mathbf{B})(OH_2)_2]^{2+}$	2.53 ± 0.04	49
$[Cu(\mathbf{C})(OH_2)_2]^{2+}$	27.1 ± 0.28	50
$[Cu(\mathbf{D})(OH_2)_2]^{2+}$	8.15 ± 1.02	50
$[Cu(\mathbf{E})(OH_2)_2]^{2+}$	6.7 ± 0.3	50

[a]Conditions used: [complex] = 150 μM, [pBR 322 plasmid] = 38 μM bp, and [HEPES] = 40 mM (pH 7.0 at 37 °C). Data were analyzed using first-order analysis, yielding k_{obs} directly. Abbreviations: **A**, 1-ethyl-4,7-*bis*(2-guanidinoethyl)-1,4,7-triazacyclononane; **B**, 1-ethyl-4,7-*bis*(3-guanidinopropyl)-1,4,7-triazacyclononane; **C**, 1-(*o*-guanidinoxylyl)-1,4,7-triazacyclononane; **D**, 1-(*m*-guanidinoxylyl)-1,4,7-triazacyclononane; and **E**, 1-(*p*-guanidinoxylyl)-1,4,7-triazacyclononane. [b][complex] = 100 μM. [c][complex] = 144 μM.

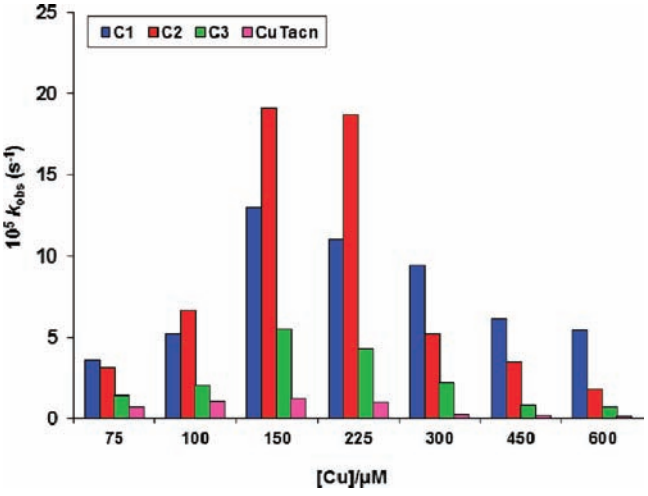

Figure 11. Concentration dependence of cleavage of pBR 322 DNA promoted by **C1**, **C2**, **C3**, and Cu^{II}-tacn in 40 mM HEPES (pH 7.0) at 37 °C over a 4 h period.

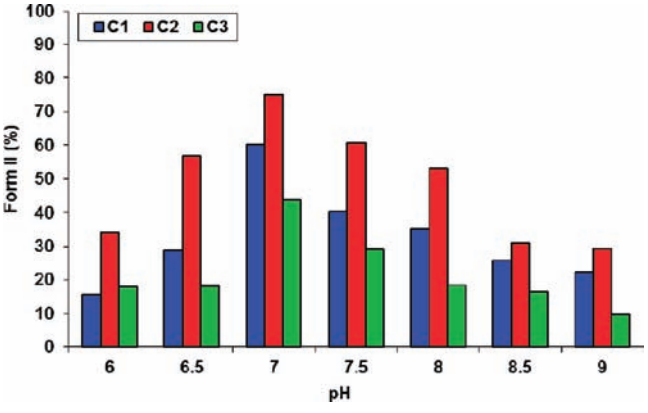

Figure 12. pH dependence of the cleavage of pBR 322 DNA promoted by **C1**, **C2**, and **C3** over a 4 h period ([DNA] = 38 μM bp, [complex] = 150 μM, and T = 37 °C).

For **C1**, the pH-dependent reactivity can be explained by considering the different protonated forms of the complex at pH 4.0–12.0 (Figure 7), each of which will have different DNA cleavage activity, with the overall cleavage activity at any pH being a cumulative effect of all the species coexisting in the solution. With an increase in pH, the concentration of the less active form of **C1**, $[Cu(L^1)(OH)]^+$, increases. A nearly saturated coordination environment around the Cu(II) center and presence of a poor nucleophile make this species least active, and as a result, reduced DNA cleavage activity is observed at higher pH. In the case of **C2** and **C3**, binuclear complexes are unlikely to play a significant role in DNA cleavage as the speciation studies (see Figure 7) indicate that the concentration of these will be very small (a few % at most) under the conditions of DNA cleavage (150–600 μM).

Drawing comparisons from other phosphate diester hydrolyzing metal diaqua complexes,[1,83,84] the Cu^{II}-aqua-hydroxo form of **C2** and **C3** should be most active in DNA cleavage. Burstyn and co-workers have reported that the first pK_a for ligated water in the $[Cu(tacn)(OH_2)_2]^{2+}$ complex is ~7.3.[80] Introduction of the guanidinium groups on the tacn ring has been found to lower this value.[85] Therefore, as the pH increases above 7, mononuclear complexes will be converted into dihydroxo complexes, $[CuL^2(OH)_2]^{2+}$ and $[CuL^3(OH)_2]^{2+}$ (see Figure 7), which leads to a decrease in the concentration of active species and a concomitant decrease in DNA cleavage rates.

The rates of DNA cleavage with [complex] (Figure 11) for **C1**–**C3** and $[Cu(tacn)(OH_2)_2]^{2+}$ were found to reach a maximum at ca. 150 μM and to then decrease as the concentration of complex is increased further. Similar reactivity profiles have been observed previously and concluded to be due to the formation of increased amounts of the hydroxo-bridged dimers, which bind DNA, blocking access of the cleavage-active monomeric species.[57,58,75,80] However, as noted previously for **C2** and **C3**, the dimer concentration is predicted to be very low under the DNA cleavage conditions. This prompts us to propose an alternative explanation for the observed behavior. The DNA cleavage experiments are conducted with an excess of metal complex, some 2–15 times the DNA base pair concentration, but the actual DNA concentration is in the nanomolar range so that [complex] is >2000 higher than [DNA] and in very large excess. Thus, it is conceivable that as [complex] increases, mononuclear forms of the complexes bind to and/or electrostatically interact with more and more of the exposed phosphate ester groups in DNA, thereby stabilizing it against cleavage.

CONCLUSION

The copper(II) complexes of three tacn-based ligands with single ethylguanidine (L^1), propylguanidine (L^2), and butylguanidine (L^3) pendant arms have been synthesized and characterized. X-ray crystallography reveal that, under basic conditions, L^1 forms a monohydroxo-bridged binuclear copper(II) complex (**C1**) in which the guanidine pendants coordinate to the copper(II) centers, forming five-membered chelate rings. In contrast, L^2 and L^3 yield mononuclear complexes (**C2** and **C3**) in which the guanidinium pendants remain protonated and do not coordinate. Complexes **C2** and **C3** are more reactive toward the simple phosphodiesters BNPP and HPNPP than the analogues featuring xylyl-linked guanidine groups, suggesting that the more flexible alkyl pendants allow the guanidinium groups to better interact with the Cu(II)-bound phosphate

dx.doi.org/10.1021/ic2019814 | *Inorg. Chem.* 2012, 51, 939–953

ester and assist with cleavage. Complex **C1** displays lower reactivity than **C2** and **C3** but is on par with the "parent" tacn complex, indicating that the coordinated guanidine may partly dissociate from the metal center to allow for substrate binding. Complexes **C1**–**C3** were all found to cleave plasmid DNA faster than $[Cu(tacn)(OH_2)_2]^{2+}$ and the Cu^{II}–tacn *bis*(alkylguanidine) complexes, indicating that they can better access the sugar–phosphate backbone and that the guanidinium groups likely act in concert with the copper(II) center to accelerate cleavage. For all three complexes, a reduction in the rate of DNA cleavage with increasing pH is attributed to the formation of hydrolytically inactive complexes. The decrease in cleavage rate with [complex], on the other hand, points to the possibility that the amount of mononuclear complex bound to DNA increases with concentration and that this stabilizes the DNA against cleavage.

■ ASSOCIATED CONTENT

Supporting Information

Crystallographic files in CIF format; table of crystallographic data (Table S01), figures showing H-bonding and unit cell lattice of complexes **C1**–**C3** (Figures S01–S03), UV–visible titration data (Figure S04); agarose gel images of DNA cleavage and kinetic profiles (Figures S05–S26 and Tables S02–S12), and histograms showing extent of DNA cleavage in presence of scavenging agents and under aerobic/anaerobic conditions (Figures S17, S19, S21, and S25). This material is available free of charge via the Internet at http://pubs.acs.org.

■ AUTHOR INFORMATION

Corresponding Author

*Fax: +61 3 9903 9582. E-mail: Bim.Graham@monash.edu (B.G.). Fax: +61 3 9905 4597. E-mail: Leone.Spiccia@monash.edu (L.S.).

■ ACKNOWLEDGMENTS

This work was supported by the Australian Research Council through the Discovery Program. L.T. is the recipient of a Monash Graduate Scholarship and Postgraduate Publication Award.

■ REFERENCES

(1) Hegg, E. L.; Burstyn, J. N. *Coord. Chem. Rev.* **1998**, *173*, 133–165.
(2) Yun, J. W.; Tanase, T.; Lippard, S. J. *Inorg. Chem.* **1996**, *35*, 7590–7600.
(3) Gomez-Tagle, P.; Yatsimirsky, A. K. *J. Chem. Soc., Dalton Trans.* **2001**, 2663–2670.
(4) Hay, R. W.; Govan, N. *Polyhedron* **1998**, *17*, 463–468.
(5) Hegg, E. L.; Burstyn, J. N. *J. Am. Chem. Soc.* **1995**, *117*, 7015–7016.
(6) Hegg, E. L.; Burstyn, J. N. *Inorg. Chem.* **1996**, *35*, 7474–7481.
(7) Hegg, E. L.; Deal, K. A.; Kiessling, L. L.; Burstyn, J. N. *Inorg. Chem.* **1997**, *36*, 1715–1718.
(8) Erkkila, K. E.; Odom, D. T.; Barton, J. K. *Chem. Rev.* **1999**, *99*, 2777–2796.
(9) Rajski, S. R.; Williams, R. M. *Chem. Rev.* **1998**, *98*, 2723–2796.
(10) Burger, R. M. *Chem. Rev.* **1998**, *98*, 1153–1170.
(11) Sherman, S. E.; Lippard, S. J. *Chem. Rev.* **1987**, *87*, 1153–1181.
(12) Cowan, J. A. *Curr. Opin. Chem. Biol.* **2001**, *5*, 634–642.
(13) Morrow, J. R.; Iranzo, O. *Curr. Opin. Chem. Biol.* **2004**, *8*, 192–200.
(14) Baker, B. F.; Lot, S. S.; Kringle, J.; Cheng-Flournoy, S.; Villiet, P.; Sasmor, H. M.; Siskowski, A. M.; Chappell, L. L.; Morrow, J. R. *Nucl. Acids. Res.* **1999**, *27*, 1547–1551.
(15) Perreault, D. M.; Ansyln, E. V. *Angew. Chem., Int. Ed.* **1997**, *36*, 432–450.
(16) Cheng, C. C.; Rokita, S. E.; Burrows, C. J. *Angew. Chem., Int. Ed.* **1993**, *32*, 277–278.
(17) Friedel, M. G.; Pieck, J. C.; Klages, J.; Dauth, C.; Kessler, H.; Carell, T. *Chem.—Eur. J.* **2006**, *12*, 6081–6094.
(18) Mancin, F.; Tecilla, P. *New J. Chem.* **2007**, *31*, 800–817.
(19) Noll, D. M.; Mason, T. M.; Miller, P. S. *Chem. Rev.* **2006**, *106*, 277–301.
(20) Hettich, R.; Schneider, H.-J. *J. Am. Chem. Soc.* **1997**, *119*, 5638–5647.
(21) Ren, R.; Yang, P.; Zheng, W.; Hua, Z. *Inorg. Chem.* **2000**, *39*, 5454–5463.
(22) Komiyama, M.; Kina, S.; Matsumura, K.; Sumaoka, J.; Tobey, S.; Lynch, V. M.; Ansyln, E. V. *J. Am. Chem. Soc.* **2002**, *124*, 13731–13736.
(23) Yang, M.-Y.; Richard, J. P.; Morrow, J. R. *Chem. Commun.* **2003**, 2832–2833.
(24) Worm, K.; Chu, F.; Matsumoto, K.; Best, M. D.; Lynch, V. M.; Ansyln, E. V. *Chem.—Eur. J.* **2003**, *9*, 741–747.
(25) Jin, Y.; Cowan, J. A. *J. Am. Chem. Soc.* **2005**, *127*, 8408–8415.
(26) An, Y.; Tong, M.-L.; Ji, L.-N.; Mao, Z.-W. *Dalton Trans.* **2006**, 2066–2071.
(27) Corneillie, T. M.; Whetstone, P. A.; Lee, K. C.; Wong, J. P.; Meares, C. F. *Bioconjugate Chem.* **2004**, *15*, 1389–1391.
(28) Qian, J.; Gu, W.; Liu, H.; Gao, F.; Feng, L.; Yan, S.; Liao, D.; Cheng, P. *Dalton Trans.* **2007**, 1060–1066.
(29) Kovari, E.; Heitker, J.; Kramer, R. *J. Chem. Soc. Chem. Commun.* **1995**, 1205–1206.
(30) Kovari, E.; Kramer, R. *J. Am. Chem. Soc.* **1996**, *118*, 12704–12709.
(31) Jubian, V.; Dixon, R. P.; Hamilton, A. D. *J. Am. Chem. Soc.* **1992**, *114*, 1120–1121.
(32) Dixon, R. P.; Geib, S. J.; Hamilton, A. D. *J. Am. Chem. Soc.* **1992**, *114*, 365–366.
(33) Jubian, V.; Veronese, A.; Dixon, R. P.; Hamilton, A. D. *Angew. Chem., Int. Ed.* **1995**, *34*, 1237–1239.
(34) Muche, M.-S.; Goebel, M. W. *Angew. Chem., Int. Ed.* **1996**, *35*, 2126–2129.
(35) Ariga, K.; Ansyln, E. V. *J. Org. Chem.* **1992**, *57*, 417–419.
(36) Ait-Haddou, H.; Sumaoka, J.; Wiskur, S. J.; Folmer-Andersen, J. F.; Ansyln, E. V. *Angew. Chem., Int. Ed.* **2002**, *41*, 4013–4016.
(37) Feng, G.; Mareque-Rivas, J. C.; de-Rosales, R. T. M.; Williams, N. H. *J. Am. Chem. Soc.* **2005**, *127*, 13470–13471.
(38) Feng, G.; Mareque-Rivas, J. C.; Williams, N. H. *Chem. Commun.* **2006**, 1845–1847.
(39) Chen, X. Q.; Wang, J. Y.; Sun, S. G.; Fan, J. L.; Wu, S.; Liu, J. F.; Ma, S. J.; Zhang, L. Z.; Peng, X. J. *Bioorg. Med. Chem. Lett.* **2008**, *18*, 109–113.
(40) He, J.; Hu, P.; Wang, Y. J.; Tong, M.-L.; Sun, H. Z.; Mao, Z.-W.; Ji, L.-N. *Dalton Trans.* **2008**, 3207–3214.
(41) Sheng, X.; Lu, X. M.; Chen, Y. T.; Lu, G.-Y.; Zhang, J. J.; Shao, Y.; Liu, F.; Xu, Q. *Chem.—Eur. J.* **2007**, *13*, 9703–9712.
(42) Shao, Y.; Sheng, X.; Li, Y.; Jia, Z. L.; Zhang, J. J.; Liu, F.; Lu, G.-Y. *Bioconjugate Chem.* **2008**, *19*, 1840–1848.
(43) Cotton, F. A.; Hazen, E. E. J.; Legg, M. *Proc. Natl. Acad. Sci. U.S.A.* **1979**, *76*, 2551–2555.
(44) Weber, D. J.; Meeker, A. K.; Mildvan, A. S. *Biochemistry* **1991**, *30*, 6103–6114.
(45) Wilcox, D. E. *Chem. Rev.* **1996**, *96*, 2435–2458.
(46) Sheng, X.; Guo, X.; Lu, M.-X.; Lu, G.-Y.; Shao, Y.; Liu, F.; Xu, Q. *Bioconjugate Chem.* **2008**, *19*, 490–498.
(47) Kim, J. H.; Youn, M. R.; Lee, Y.-A.; Kim, J. M.; Kim, S. K. *Bull. Korean Chem. Soc.* **2007**, *28*, 263–270.
(48) Iranzo, O.; Elmer, T.; Richard, J. P.; Morrow, J. R. *Inorg. Chem.* **2003**, *42*, 7737–7746.

(49) Tjioe, L.; Joshi, T.; Brugger, J.; Graham, B.; Spiccia, L. *Inorg. Chem.* **2011**, *50*, 621−635.
(50) Tjioe, L.; Meininger, A.; Joshi, T.; Graham, B.; Spiccia, L. *Inorg. Chem.* **2011**, *50*, 4327−4339.
(51) Kimura, S.; Bill, E.; Bothe, E.; Weyhermuller, T.; Wieghardt, K. *J. Am. Chem. Soc.* **2001**, *123*, 6025−6039.
(52) Brown, D. M.; Usher, D. A. *J. Chem. Soc.* **1965**, 6558−6564.
(53) Tsang, J. S.; Neverov, A. A.; Brown, R. S. *J. Am. Chem. Soc.* **2003**, *125*, 1559−1566.
(54) Brugger, J. *Comput. Geosci.* **2007**, *33*, 248−261.
(55) Brugger, J.; McPhail, D. C.; Black, J.; Spiccia, L. *Geochim. Cosmochim. Acta* **2001**, *65*, 2691−2708.
(56) Liu, W.; Etschmann, B.; Brugger, J.; Spiccia, L.; Foran, G.; McInnes, B. *Chem. Geol.* **2006**, *231*, 326−349.
(57) Fry, F.; Fischmann, A. J.; Belousoff, M. J.; Spiccia, L.; Brugger, J. *Inorg. Chem.* **2005**, *44*, 941−950.
(58) Belousoff, M. J.; Duriska, M. B.; Graham, B.; Batten, S. R.; Moubaraki, B.; Murray, K. S.; Spiccia, L. *Inorg. Chem.* **2006**, *47*, 3746−3755.
(59) Sheldrick, G. M. *SHELXL-97*; University of Gottingen: Gottingen, Germany, 1997.
(60) Sheldrick, G. M. *SHELXS-97*; University of Gottingen: Gottingen, Germany, 1997.
(61) Schwindinger, W. F.; Fawcett, T. G.; Lalancette, R. A.; Potenza, J. A.; Schugar, H. J. *Inorg. Chem.* **1980**, *19*, 1379−1381.
(62) Addison, A. W.; Rao, T. N.; Reedjik, J.; Rijin, J. V.; Verschoor, G. C. *J. Chem. Soc., Dalton Trans.* **1984**, 1349−1356.
(63) Di Vaira, M.; Mani, F.; Stoppioni, P. *Inorg. Chim. Acta* **2000**, *303*, 61−69.
(64) Graham, B.; Spiccia, L.; Fallon, G. D.; Hearn, M. T. W.; Mabbs, F. E.; Moubaraki, B.; Murray, K. S. *J. Chem. Soc., Dalton Trans.* **2002**, 1226−1232.
(65) Chaudhuri, P.; Ventur, D.; Wieghardt, K.; Peters, E., -M.; Peters, K.; Simon, A. *Angew. Chem., Int. Ed.* **1985**, *24*, 57−59.
(66) Elliot, D. J.; Martin, L. L.; Taylor, M. R. *Acta Crystallogr., Sect. C* **1998**, *54*, 1259−1261.
(67) Farrugia, L. J.; Lovatt, P. A.; Peacock, R. D. *J. Chem. Soc., Dalton Trans.* **1997**, 911−912.
(68) Graham, B.; Hearn, M. T. W.; Junk, P. C.; Kepert, C. M.; Mabbs, F. E.; Moubaraki, B.; Murray, K. S.; Spiccia, L. *Inorg. Chem.* **2001**, *40*, 1536−1543.
(69) Farrugia, L. J.; Lovatt, P. A.; Peacock, R. D. *Inorg. Chim. Acta* **1996**, *246*, 343−348.
(70) Evans, A. J.; Watkins, S. E.; Craig, D. C.; Colbran, S. B. *J. Chem. Soc., Dalton Trans.* **2002**, 983−994.
(71) Mahapatra, S.; Halfen, J. A.; Wilkinson, E. C.; Pan, G.; Wang, X.; Young, V. G. J.; Cramer, C. J.; Que, L. J.; Tolman, W. B. *J. Am. Chem. Soc.* **1996**, *118*, 11555−11574.
(72) Fry, F.; Spiccia, L.; Jensen, P.; Moubaraki, B.; Murray, K. S.; Tieknik, E. D. T. *Inorg. Chem.* **2003**, *42*, 5594−5603.
(73) Brudenell, S. J.; Spiccia, L.; Tieknik, E. D. T. *Inorg. Chem.* **1996**, *35*, 1974−1979.
(74) Tei, L.; Bencini, A.; Blake, A. J.; Lippolis, V.; Perra, A.; Valtancoli, B.; Wilson, C.; Schroder, M. *Dalton Trans.* **2004**, 1934−1944.
(75) Belousoff, M. J.; Battle, A. R.; Graham, B.; Spiccia, L. *Polyhedron* **2007**, *26*, 344−355.
(76) Kruger, P. E.; Moubaraki, B.; Fallon, G. D.; Murray, K. S. *J. Chem. Soc., Dalton Trans.* **2000**, 713−718.
(77) Bleaney, B.; Bowers, K. D. *Proc. R. Soc* **1952**, *214*, 451−465.
(78) Koval, I. A.; van der Schilden, K.; Schuitema, A. M.; Gamez, P.; Belle, C.; Pierre, J.-L.; Luken, M.; Krebs, B.; Roubeau, O.; Reedjik, J. *Inorg. Chem.* **2005**, *44*, 4372−4382.
(79) Draper, N. R.; Smith, H. *Applied Regression Analysis*; Wiley: New York, 1998.
(80) Deck, K. M.; Tseng, T. A.; Burstyn, J. N. *Inorg. Chem.* **2002**, *41*, 669−677.
(81) Bazzicalupi, C.; Bencini, A.; Bonaccini, C.; Giorgi, C.; Gratteri, P.; S., M.; Palumbo, M.; Simionato, A.; Sgrignani, J.; Sissi, C.; Valtancoli, B. *Inorg. Chem.* **2008**, *47*, 5473−5484.
(82) Eigner, J.; Boedtker, H.; Michaels, G. *Biochim. Biophys. Acta* **1961**, *51*, 165−168.
(83) Chin, J.; Zou, X. *J. Am. Chem. Soc.* **1988**, *110*, 223−225.
(84) Chin, J.; Banaszczyk, M.; Jubian, V.; Zou, X. *J. Am. Chem. Soc.* **1989**, *111*, 186−190.
(85) Aoki, S.; Iwaida, K.; Hanamoto, N.; Shiro, M.; Kimura, E. *J. Am. Chem. Soc.* **2002**, *124*, 5256−5257.